Antiangiogenic Effectiveness of the Urokinase Receptor-Derived Peptide UPARANT in a Model of Oxygen-Induced Retinopathy

Massimo Dal Monte,[1] Sara Rezzola,[2] Maurizio Cammalleri,[1] Mirella Belleri,[2] Filippo Locri,[1] Lucia Morbidelli,[3] Michela Corsini,[2] Giuseppe Paganini,[2] Francesco Semeraro,[4] Anna Cancarini,[4] Dario Rusciano,[5] Marco Presta,[2] and Paola Bagnoli[1]

[1]Department of Biology, University of Pisa, Pisa, Italy
[2]Department of Molecular and Translational Medicine, University of Brescia, Brescia, Italy
[3]Department of Life Sciences, University of Siena, Siena, Italy
[4]Department of Ophthalmology, University of Brescia, Brescia, Italy
[5]Sooft Italia Spa, Montegiorgio, Italy

Correspondence: Paola Bagnoli, Department of Biology, University of Pisa, Via San Zeno, 31, 56127 Pisa, Italy; paola.bagnoli@unipi.it.
Marco Presta, Department of Molecular and Translational Medicine, University of Brescia, Viale Europa 11, 25123 Brescia, Italy; marco.presta@unibs.it.

MDM, SR, and MC contributed equally to the work presented here and should therefore be regarded as equivalent authors.

Submitted: December 23, 2014
Accepted: March 5, 2015

Citation: Dal Monte M, Rezzola S, Cammalleri M, et al. Antiangiogenic effectiveness of the urokinase receptor-derived peptide UPARANT in a model of oxygen-induced retinopathy. *Invest Ophthalmol Vis Sci*. 2015;56:2392–2407. DOI:10.1167/iovs.14-16323

Purpose. Pharmacologic control of neovascularization is a promising approach for the treatment of retinal angiogenesis. UPARANT, an inhibitor of the urokinase-type plasminogen activator receptor (uPAR), inhibits VEGF-driven angiogenesis in vitro and in vivo. This study investigates for the first time the effectiveness of UPARANT in counteracting pathologic neovascularization in the retina.

Methods. Murine retinal fragments and a mouse model of oxygen-induced retinopathy (OIR) were used. In mice with OIR, UPARANT-treated retinas were analyzed for avascular area and neovascular tuft formation. Levels of transcription and proangiogenic factors were determined. UPARANT effects on the blood–retinal barrier (BRB), visual function, retinal cytoarchitecture, and inflammatory markers were also assessed. Human umbilical vein endothelial cells (HUVECs) and chick embryo chorioallantoic membrane (CAM) in which angiogenesis was induced by the vitreous fluid from patients with proliferative diabetic retinopathy (PDR) were also used.

Results. UPARANT reduced VEGF-induced angiogenesis in retinal fragments. In mice with OIR, UPARANT decreased neovascular response, VEGF, and VEGF receptor-2 activity. Transcription factors regulating VEGF expression were also reduced. UPARANT restored BRB integrity, recovered visual loss, and reduced levels of inflammatory markers. Restored electroretinogram does not involve any rescue in the retinal cytoarchitecture. Finally, UPARANT blocked PDR vitreous fluid–induced angiogenesis in HUVEC and CAM assays.

Conclusions. The finding that UPARANT is effective against neovascularization may help to establish uPAR as a target in the treatment of proliferative retinopathies. The potential application of UPARANT in retinal diseases is further supported by UPARANT capacity to counteract the angiogenic activity of PDR vitreous fluid.

Keywords: VEGF, PDR vitreous fluid, retina

The urokinase-type plasminogen activator (uPA) and its receptor (uPAR) form a system that plays an important role in angiogenesis.[1] In particular, there are indications that uPAR is implicated in the first phases of VEGF-initiated angiogenesis by triggering extracellular matrix degradation and driving endothelial cell migration.[2,3] In addition, uPAR may also drive angiogenesis in a protease-independent manner.[4]

Among diseases involving pathologic neovascularization, proliferative retinopathies including retinopathy of prematurity (ROP), diabetic retinopathy (DR), and age-related macular degeneration (AMD) are of particular importance. Treatment for ROP is typically laser ablation of the peripheral retina although anti-VEGF drugs may also be used. In this respect, the larger concerns are related to whether the anti-VEGF compounds act systemically[5] and are damaging to the immature retina.[6] Treatment for DR and AMD is based on anti-VEGF therapies, which may pose several concerns. In particular, they require intravitreal injections at a relatively high frequency, which may lead to adverse side effects such as ocular inflammation and endophthalmitis. In addition, anti-VEGF therapies show a loss of efficacy as the disease progresses, leaving patients at late retinopathy stages with limited treatment options.[7]

In search for novel therapies against pathologic angiogenesis, peptide analogues targeting uPAR have been developed. Indeed, uPAR is an important component of the angiogenic response in the retina. In fact, uPAR expression is upregulated in concomitance with neovascular pathology in the mouse retina in which uPAR is localized to endothelial cells lining the superficial vessels and the new capillaries extending into the vitreous cavity.[8] In the bovine retina, uPAR is expressed by endothelial cells,[9] whereas in the human retina, uPAR is

expressed by pigment epithelial cells, which modulates proliferation and invasiveness in response to citokine.[10] In rodent models of neovascular pathologies, uPAR deletion or uPAR blockade with Å6, a peptide inhibitor, drastically reduces either retinal or choroidal neovascularization and ameliorates blood–retinal barrier (BRB) dysfunction.[8,11,12] However, peptide inhibitors of uPAR display some pharmacokinetic drawbacks common to peptides as they are susceptible to proteolytic degradation and are rapidly cleared from the circulation; therefore, new peptide uPAR inhibitors with optimized properties for therapeutic applications have been developed.

Among the series of newly synthesized analogues, the tetrapeptide Ac-L-Arg-Aib-L-Arg-L-Cα(Me)Phe-NH2, named UPARANT, displays strong inhibition of endothelial cell migration, long-time resistance to enzymatic digestion, and high stability in blood and plasma. Using angiogenic assays both in vitro and in vivo, Carriero et al.[13] have demonstrated that UPARANT blocks uPAR-dependent cell signaling by interfering with the complex cross talk involving uPAR, formyl peptide receptors (FPRs), and integrins.

Mechanistically, UPARANT inhibits VEGF-driven angiogenesis by preventing FPR activation, thus inhibiting only a part of the VEGF signaling. This suggests a potentially wider, but still target-specific activity for UPARANT.[13] On the other hand, a direct interaction between UPARANT and VEGF cannot be excluded. In this respect, uPAR inhibition or *uPAR* gene deletion results in decreased VEGF expression in tumor models.[14–16] Reduced VEGF levels consequent to uPAR deletion appear to depend on reduced activity of hypoxia inducible factor 1 (HIF-1) and signal transduction and activator of transcription 3 (STAT3) in glioma cells.[14]

No information is available on the effectiveness of UPARANT in counteracting angiogenesis-driven diseases in the retina.

In the present study, we used a mouse model of oxygen-induced retinopathy (OIR). This model is widely used as a surrogate for investigating the pathogenesis of ROP although its use can be extended to studies of ischemic retinopathies and their related treatments.[17] In OIR mice, the retina is characterized by capillary disappearance from the central area followed by abnormal formation of new blood vessels in the midperipheral region, which results from a drastic upregulation of proangiogenic factors including VEGF.[18] There is also evidence that inflammatory responses to ischemia may play a pivotal role in neovascular pathologies and may contribute to upregulation of proangiogenic factors.[19] In addition, OIR retinas are characterized by BRB dysfunction presumably caused by VEGF upregulation that would act as a permeability factor.[20] Moreover, OIR mice are characterized by profound visual dysfunctions as determined by electroretinogram (ERG), a useful tool to determine receptor/postreceptor function in the retina.[21–24] Preliminarily, we evaluated the effects of UPARANT on VEGF-induced angiogenesis using retinal fragments in which endothelial sprouts originate from mature and quiescent retinal vessels.[25] Then, we investigated the effectiveness of UPARANT in counteracting retinal pathologic vascularization. In addition, mechanisms underlying antiangiogenic action of UPARANT were also studied by evaluating the effects of UPARANT on HIF-1 and STAT3 activity. Moreover, we assessed the effects of UPARANT on BRB, ERG, retinal cytoarchitecture, and inflammatory markers. Finally, the antiangiogenic effectiveness of UPARANT was assessed in sprouting assays including human umbilical vein endothelial cells (HUVECs) and chick embryo chorioallantoic membrane (CAM) in which sprouting was induced by the vitreous fluid collected from patients with proliferative diabetic retinopathy (PDR). This experimental procedure determines the effectiveness of UPARANT in counteracting angiogenic processes elicited by a milieu that contains high levels of proangiogenic agents[26–28] and induces retinal endothelial cell proliferation by acting as a human eye–derived proangiogenic factor.[29–32]

Materials and Methods

UPARANT and fluorescein-labeled UPARANT (FITC-UPARANT) were synthesized as described[13] and provided by V Pavone (University of Naples, Naples, Italy). All reagents used in peptide synthesis were of the purest analytical grade. Medium M199 and fetal calf serum (FCS) were from Gibco Life Technologies (Grand Island, NY, USA). The serum-free endothelial cell basal medium was from Clonetics (Walkersville, MD, USA). Human recombinant VEGF (VEGF-A_{165} isoform) was provided by K. Ballmer-Hofer (PSI, Villigen, Switzerland). The protease inhibitor cocktail Complete and the in situ cell death detection kit were obtained from Roche Applied Science (Indianapolis, IN, USA). The phosphatase inhibitor cocktail; the rabbit polyclonal antibodies directed to the principal splice variants of VEGF-A (cat. sc-507), VEGF receptor (VEGFR)-2 (cat. sc-504), STAT3 (cat. sc-428), albumin (cat. sc-50536), Bax (cat. sc-493), and Bcl-2 (cat. sc-492); the mouse monoclonal antibody directed to the phosphorylated form of VEGFR-2, pVEGFR-2 (cat. sc-16628); the α subunit of HIF-1 (HIF-1α) (cat. sc-53546) and the phosphorylated form of STAT3 (pSTAT3; cat. sc-8059); and the mouse anti-rabbit HRP-labeled secondary antibody (cat. sc-2357) were from Santa Cruz Biotechnologies (Dallas, TX, USA). The rat cluster of differentiation 31 (CD31) monoclonal antibody (cat. 550274) and the mouse monoclonal antibody directed to cytochrome c (cyt c, cat. 556433) were obtained from BD Biosciences (San Diego, CA, USA). The secondary antibody AlexaFluor 488 was from Molecular Probes (Eugene, OR, USA). The polyvinylidene difluoride (PVDF) membrane was obtained from Bio-Rad Laboratories, Inc. (Hercules, CA, USA). The enhanced chemiluminescence reagent was obtained from Millipore Corp. (Billerica, MA, USA). The rabbit polyclonal antibody directed to occludin (cat. 71-1500) was from Zymed Laboratories, Inc. (South San Francisco, CA, USA). The RNA purification and RT-PCR kits were obtained from Qiagen, Inc. (RNeasy Mini Kit, QuantiTect Reverse Transcription Kit, and SYBR Green PCR Kit; Valencia, CA, USA). Polymerase chain reaction (PCR) primer sets were from Eurofins Genomics (Ebersberg, Germany). All other chemicals were obtained from Sigma-Aldrich Corp. (St. Louis, MO, USA).

Animals

Procedures involving animals were carried out in agreement with the ARVO Statement for the Use of Animals in Ophthalmic and Vision Research and in compliance with the Italian guidelines for animal care (DL 116/92) and the European Communities Council Directive (86/609/EEC). Procedures were approved by the Ethical Committee in Animal Experiments of the University of Pisa. Animals were kept in a regulated environment (23 ± 1°C, 50% ± 5% humidity) with a 12-hour light/dark cycle (lights on at 8 AM) with food and water ad libitum. All efforts were made to reduce both animal suffering and the number of animals used.

Ex Vivo Murine Retinal Angiogenesis (EMRA) Assay

Angiogenesis assay was performed in retinas explanted from C57BL/6 mice (Charles River Laboratories, Inc., Wilmington, MA, USA) aged 4 to 5 weeks in agreement with previous work.[25] Briefly, animals ($n = 15$) were killed, and isolation of the retinas

was performed. The isolated retinas were cut to obtain four equal quadrants, and fragments were embedded in 3D fibrin gel after overnight incubation in serum-free medium. Then, culture medium containing increasing concentrations of UPARANT (1 pM–1 nM) was added on top of the gel in the presence of 75 ng·mL^{-1} VEGF and 10 μg·mL^{-1} aprotinin. After 7 days, vessel sprouts were counted under a microscope (Axiovert 200M; Carl Zeiss Vision GmbH, München-Hallbergmoos, Germany). After statistical analysis, data from the different experiments were plotted and averaged on the same graph.

Model of Oxygen-Induced Retinopathy

In the model of OIR, litters of mice pups (C57BL/6, $n = 92$) with their nursing mothers were exposed in an infant incubator to high oxygen concentrations (75% ± 2%) between postnatal day (PD)7 and 12, before returning to room air between PD12 and PD17.[33] Oxygen was checked twice daily with an oxygen analyzer (Pro-Custom Elettronica SRL, Milano, Italy). Individual litters were reared in either oxygen or room air (controls). The pharmacologic treatment was performed in animals anesthetized by intraperitoneal injection of Avertin (1.2% tribromoethanol and 2.4% amylene hydrate in distilled water, 0.02 mL·g body weight^{-1}). The data were collected from both males and females, and the results combined, as there was no apparent sex difference.

Intravitreal Injection of UPARANT

At PD12 and PD15, mice were anesthetized by intraperitoneal injection of avertin and subjected to intravitreal injection of 1 μL UPARANT dissolved in sterile PBS, at 0.0015, 0.015, 0.15, or 1.5 μg μL^{-1}. Intravitreal injections were performed using a microsyringe (NanoFil syringe; World Precision Instruments, Inc., Sarasota, FL, USA). UPARANT was injected into the left eye, while the right eye was injected with PBS and served as a control. Mice were killed at PD17. For electroretinographic measurements, mice were intravitreally injected with UPARANT or PBS in both eyes.

Immunohistochemistry and Quantitative Analysis

The retinal vasculature was visualized in whole retinas using antibodies directed to CD31, an endothelial cell marker.[34] Immunohistochemistry on retinal whole mounts and quantitative analysis of preretinal neovascular tuft formation, vascular and avascular areas, were performed in line with previous works.[35–38] Dissected retinas were immersion fixed for 1.5 hours in 4% paraformaldehyde in 0.1 M phosphate buffer (PB) at 4°C, transferred to 25% sucrose in 0.1 M PB, and stored at 4°C. The retinal whole mounts were freeze thawed and incubated for 72 hours at 4°C in the CD31 antibody (1:50 in 0.1 M PB containing 0.5% Triton X-100). The whole mounts were then incubated for 48 hours at 4°C with AlexaFluor 488–conjugated secondary antibody (1:200 in 0.1 M PB). Finally, they were rinsed in 0.1 M PB, mounted on gelatin-coated glass slides, and cover slipped with a 0.1-M PB–glycerine mixture. Images of the retinal vasculature were acquired with a microscope equipped with epifluorescence (Eclipse E800; Nikon Corp., Amsterdam, The Netherlands) through a digital photocamera (DS-Fi1c camera; Nikon Corp.). Electronic images were processed using image-editing software (Adobe Photoshop; Adobe Systems, Inc., Mountain View, CA, USA) to create whole retina montages. Subsequent quantification was performed on these montages. For each experimental condition, quantitative data originated from six retinas from six different mice. After statistical analysis, averaged data were plotted on the same graph.

Western Blot Analysis

Retinas ($n = 45$) were sonicated in 10 mM Tris-HCl (pH 7.6) containing 5 mM EDTA, 3 mM EGTA, 250 mM sucrose, protease, and phosphatase inhibitor cocktails and centrifuged at 22,000*g* for 30 minutes at 4°C. The supernatants were used to detect VEGF, HIF-1α, STAT3, pSTAT3, albumin, Bax, Bcl-2, and cytochrome c. Pellets were resuspended in 20 mM HEPES, pH 7.4, containing 150 mM NaCl, 5 mM EDTA, 3 mM EGTA, 4 mg·mL^{-1} n-dodecyl-β-maltoside, protease, and phosphatase inhibitor cocktails, and centrifuged at 22,000*g* for 30 minutes at 4°C. The supernatants were used to detect VEGFR-2, pVEGFR-2, and occludin. Protein concentration was determined using a fluorometer (Qubit; Invitrogen, Carlsbad, CA, USA). Aliquots of each sample containing equal amounts of protein (30 μg) were subjected to SDS-PAGE. We used β-actin as the loading control. The gels were transblotted onto PVDF membrane, and the blots were blocked in 3% skim milk for 1 hour at room temperature. Blots were then incubated overnight at 4°C with rabbit polyclonal antibodies directed to VEGF (1:200); VEGFR-2 (1:200); STAT3 (1:200); albumin (1:200); occludin (1:250); Bax (1:100); and Bcl-2 (1:100); or mouse monoclonal antibodies directed to pVEGFR-2 (1:100); HIF-1α (1:200); pSTAT3 (1:200); and cytochrome c (1:500). The same membrane was reblotted with a mouse monoclonal antibody directed to β-actin (1:10,000). Finally, blots were incubated for 1 hour at room temperature with a mouse anti-rabbit horseradish peroxidase–labeled secondary antibody (1:5000) or a rabbit anti-mouse horseradish peroxidase–labeled secondary antibody (1:25,000) and developed with the enhanced chemiluminescence reagent. Images were acquired (ChemiDoc XRS^{+}; Bio-Rad Laboratories, Inc.), and the optical density (OD) of the bands was evaluated (Image Lab 3.0 software; Bio-Rad Laboratories, Inc.). The data were normalized to the level of β-actin, VEGFR-2, or STAT3, as appropriate. All experiments were run in duplicate. After statistical analysis, data from the different experiments were plotted and averaged on the same graph.

Measurement of Retinal Vascular Leakage

Blood–retinal barrier leakage was evaluated qualitatively using Evans blue dye. The use of this dye in the evaluation of BRB leakage has been observed to pose several problems,[39] although these problems are particularly relevant only for quantitative evaluation of BRB leakage.[40] After the mice were deeply anesthetized with avertin, Evans blue dye, dissolved in normal saline (30 mg·mL^{-1}), was injected into the left ventricle and allowed to circulate through the body for 5 minutes. After the enucleated eyes were fixed in 4% paraformaldehyde, the retinas were flat mounted and examined with a fluorescence microscope (Eclipse E800; Nikon Corp.), and images were acquired (DS-Fi1c camera; Nikon Corp.). For each experimental condition, six retinas from six different mice were used.

Electroretinography

Retinal function was examined with scotopic full-field ERG recorded from PD17 mice. The electrophysiologic signals were recorded as previously described.[37,41] Briefly, mice were dark adapted overnight and anesthetized by intraperitoneal injection of avertin. Pupils were dilated with 0.5% atropine. Mixed (rod and cone) responses were evoked by flashes of different light intensities ranging from −3.4 to 1 log cd-s.m^{-2} generated through a Ganzfeld stimulator (Biomedica Mangoni, Pisa, Italy). The amplitude of the a-wave was measured at a fixed time of 8 ms after stimulus onset to minimize contamination from non-

photoreceptoral contributions.[42] The b-wave amplitude was measured from the trough of the a-wave to the peak of the b-wave. Of the five oscillatory potentials (OPs) that can generally be isolated from the mouse ERG, only OP2, OP3, and OP4 were analyzed as OP1 and OP5 could not be accurately measured at PD17.[43] For each OP, the trough-to-peak amplitude was measured, and the amplitudes of each wavelet were added to create the sum OPs (SOPs).[44] Mean amplitudes of ERG responses were plotted as a function of increasing light intensities. For each experimental condition, ERG analysis was performed on six mice.

Retinal Sections and TUNEL Staining

Enucleated eyes were immersion fixed for 1.5 hours in 4% paraformaldehyde in 0.1 M PB at 4°C, transferred to 25% sucrose in 0.1 M PB, and stored at 4°C. Fixed eyes were embedded in Killik medium (Bio Optica Milano, Milan, Italy), frozen at −20°C, serially sectioned at 10 μm on a cryostat, mounted on gelatin-coated slides, and stored at −20°C. An in situ cell death detection kit (Roche Applied Science) was used to identify apoptotic profiles by TUNEL technique according to the manufacturer's instructions. The slides were coverslipped in a 0.1 M PB–glycerin mixture containing 0.5 μg mL^{-1} of 4′,6-diamidino-2-phenylindole (DAPI). The retinal layer thickness was evaluated in selected sections. The fluorescent TUNEL staining was used to calculate an index of cell death in the nuclear layers of the retina. Images of both the TUNEL and the DAPI stainings were acquired with a microscope (Eclipse E800; Nikon Corp.) using a digital camera (DS-Fi1c; Nikon Corp.).

Isolation of RNA and cDNA Preparation

Dissected retinas were immediately frozen in liquid nitrogen and stored at −80°C until analysis. Total RNA was extracted (RNeasy Mini Kit; Qiagen, Inc.), purified, resuspended in RNase-free water, and quantified using a fluorometer (Invitrogen). First-strand cDNA was generated from 1 μg total RNA (Qiagen, Inc.).

Quantitative RT-PCR

To evaluate gene expression, quantitative real-time RT-PCR (QPCR) experiments were performed on a total of 20 retinas using a kit (Qiagen, Inc.). Quantitative real-time RT-PCR primer sets for inflammatory markers including tumor necrosis factor (TNF)-α, interleukin (IL)-1β, IL-6, inducible nitric oxide synthase (iNOS), intercellular adhesion molecule (ICAM)-1, and glial fibrillary acidic protein (GFAP) were obtained from previously published studies or from PrimerBank,[45–47] while the primer set for Rpl13a was obtained from RTPrimerDB.[48] Forward and reverse primers were chosen to hybridize to unique regions of the appropriate gene sequence. Their sequences were as follows: TNF-α forward 5′-GCCTCTTCTCA TTCCTGCTT-3′, TNF-α reverse 5′-CTCCTCCACTTGGTGGTT TG-3′, IL-1β forward 5′-TCCTTGTGCAAGTGTCTGAAGC-3′, IL-1β reverse 5′-ATGAGTGATACTGCCTGCCTGA-3′, IL-6 forward 5′-TCTGCAAGAGACTTCCATCCAGT-3′, IL-6 reverse 5′-TCTGCAACTGCATCATCGTTGT-3′, iNOS forward 5′-GGCAAA CCCAAGGTCTACGTT-3′, iNOS reverse 5′-TCGCTCAAGTTCA GCTTGGT-3′, ICAM-1 forward 5′-CGCTGTGCTTTGAGAACT GTG-3′, ICAM-1 reverse 5′-ATACACGGTGATGGTAGCGGA-3′, GFAP forward 5′-CGGAGACGCATCACCTCTG-3′, GFAP reverse 5′-AGGGAGTGGAGGAGTCATTCG-3′, Rpl13a forward 5′-CACTCTGGAGGAGAAACGGAAGG-3′, and Rpl13a reverse 5′-GCAGGCATGAGGCAAACAGTC-3′. Amplification efficiency was close to 100% for each primer pair (Opticon Monitor 3 software; Bio-Rad Laboratories, Inc.). Target genes were run concurrently with Rpl13a, a constitutively expressed gene encoding a ribosomal protein that is a component of the 60S subunit[49]; Rpl13a is a stable housekeeping gene in OIR retinas.[37] Samples were compared using the relative threshold cycle (Ct Method).[50] The increase or decrease (×-fold) was determined relative to a control after normalizing to Rpl13a. All reactions were run in triplicate. After statistical analysis, the data from the different experiments were plotted and averaged in the same graph.

Preparation of Human Vitreous Fluid Samples

This study enrolled patients ($n = 18$) with PDR who underwent a pars plana vitrectomy at the Clinics of Ophthalmology of the University of Brescia, Italy. Collection and analysis of human samples were approved by the internal review board of the Spedali Civili of Brescia and followed the tenets of the Declaration of Helsinki. In some patients, intravitreal injection of bevacizumab or ranibizumab was performed 10 to 15 days prior to vitrectomy. During vitrectomy, samples of vitreous fluid were collected under sterile conditions by suction with a syringe connected to the vitrectomy instruments before starting the infusion of saline solution. Samples were therefore pure and undiluted by any substance. Vitreous fluid samples were stored at −80°C. After thawing, samples were clarified by centrifugation. Samples from six different patients were pooled together obtaining three different pools, and angiogenesis assays were performed on pooled material. In vitreous fluid, protein concentration was assessed using a protein assay reagent (Bio-Rad Laboratories, Inc.).

HUVEC Sprouting Assay

Human umbilical vein endothelial cells were isolated from umbilical cords, used at early (I–IV) passages, and grown on plastic surface coated with porcine gelatin in M199 medium supplemented with 20% FCS, endothelial cell growth factor (100 μg·mL^{-1}), and porcine heparin (100 μg·mL^{-1}). Sprouting of HUVEC aggregates embedded in fibrin gel was analyzed as described.[51] Briefly, spheroids were stimulated with 30 ng·mL^{-1} VEGF or with PDR vitreous fluid in the presence of increasing concentrations of UPARANT (1 pM–1 nM). After 24 hours, growing cell sprouts were counted using a microscope (Carl Zeiss Vision GmbH). After statistical analysis, data from the different experiments were plotted and averaged on the same graph.

Chick Embryo CAM Assay

Alginate beads (5 μL) containing 0.1 μg VEGF or PDR vitreous fluid in the presence of increasing amounts of UPARANT (0.01–1 μg) were placed on top of the CAM of fertilized white leghorn chicken eggs ($n = 72$) at day 11 of incubation.[52] After 3 days, newly formed microvessels converging toward the implant were counted at ×5 magnification using a STEMI SR stereomicroscope (Carl Zeiss Vision GmbH). After statistical analysis, data from the different experiments were plotted and averaged on the same graph.

FITC-UPARANT Binding Assay

To assess whether PDR vitreous fluid may interfere with the binding of UPARANT to HUVECs and its consequent internalization, cells were incubated at 37°C with 0.15 mM FITC-UPARANT in the absence or in the presence of a 10-fold molar excess of unlabeled UPARANT or with PDR vitreous fluid. After 60 minutes, cells were extensively washed with PBS, nuclear

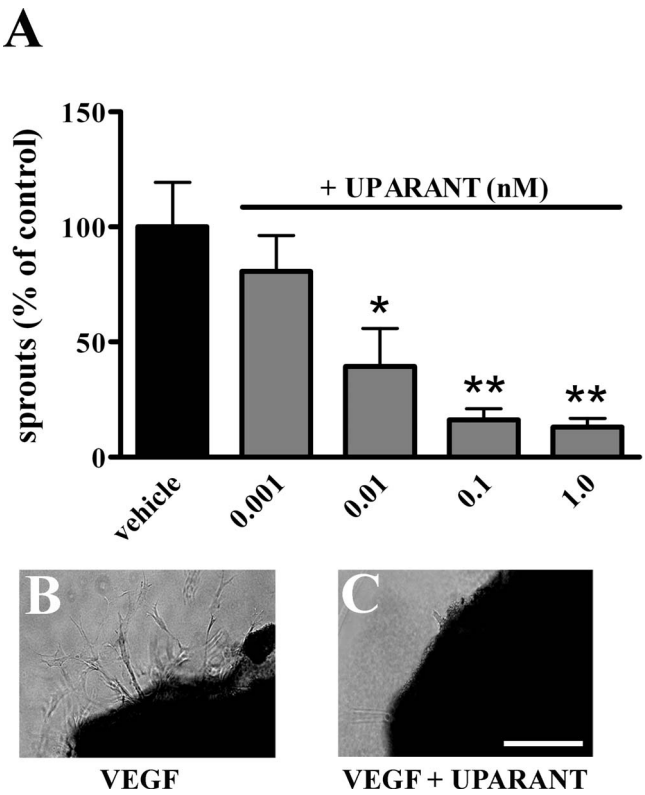

FIGURE 1. UPARANT inhibits angiogenesis in the EMRA assay. Retinal fragments were embedded in fibrin gel and incubated in the presence of VEGF (75 ng mL^{-1}) in combination with vehicle (PBS) or increasing concentrations of UPARANT. After 7 days, vessel sprouts invading the surrounding fibrin matrix were counted. (**A**) UPARANT dose-dependently reduced the formation of vessel sprouts (*$P < 0.01$ and **$P < 0.001$ versus vehicle treated; ANOVA). Each column represents the mean ± SEM of data from 30 fragments. (**B**, **C**) Representative images of retinal fragments treated with VEGF in the presence of either vehicle or 0.1-nM UPARANT. *Scale bar*: 200 μm.

counterstained with DAPI, and photographed using an epifluorescence microscope (Carl Zeiss Vision GmbH).

Data Analysis

All data were analyzed by the Shapiro-Wilk test to verify their normal distribution. Statistical significance was evaluated with commercial software (GraphPad Prism 4; GraphPad Software, San Diego, CA, USA) using one-way ANOVA followed by Newman-Keuls multiple comparison posttest. The results were expressed as mean ± SEM of the indicated n values. Differences with $P < 0.05$ were considered significant.

RESULTS

UPARANT Reduces VEGF-Induced Angiogenesis in the EMRA Assay

In preliminary experiments, we used a novel assay recently established by Rezzola et al.[25] in order to test antiangiogenic effectiveness of UPARANT in a retina-related assay. As shown in Figure 1, UPARANT dose-dependently inhibited VEGF-induced neovascularization. In particular, vessel sprouts were not affected by UPARANT at 0.001 nM, while they were reduced by approximately 60% ($P < 0.01$), 84% ($P < 0.001$), and 87% ($P < 0.001$) by UPARANT at 0.01, 0.1, and 1 nM, respectively.

UPARANT Reduces Retinal Neovascularization, VEGF Levels, and the Expression of Transcription Factors in OIR Mice

We used CD31 immunohistochemistry to evaluate retinal angiogenesis after the administration of increasing doses of UPARANT. Figure 2 is representative of the vascular pattern observed at PD17 in retinas of control mice (Fig. 2A) and in vehicle-treated retinas of OIR mice (Fig. 2B) in which a large avascular area could be seen in the central zone and an excessive regrowth of abnormal superficial vessels leading to preretinal neovascular tufts was observed in the midperipheral retina. No differences in the extent of the avascular area (red contours) were observed between vehicle- and UPARANT-treated retinas, whereas the area occupied by neovascular tufts (yellow contours) was evidently reduced in a dose-dependent manner (Figs. 2C–F). The quantitative analysis confirmed that UPARANT did not affect the avascular area (Fig. 2G), whereas it dose-dependently reduced the area occupied by neovascular tufts (Fig. 2H). In particular, the neovascular tuft area was not affected by UPARANT at 0.0015 μg μL^{-1}, while it was reduced by approximately 62% ($P < 0.001$), 75% ($P < 0.001$), and 85% ($P < 0.0001$) by UPARANT at 0.015, 0.15, and 1.5 μg μL^{-1}, respectively.

As shown in Figures 3A and 3B, UPARANT dose-dependently reduced retinal levels of VEGF. In particular, VEGF levels were not affected by UPARANT at 0.0015 and 0.015 μg μL^{-1}, while they were reduced by approximately 49% ($P < 0.01$) and 63% ($P < 0.001$) by UPARANT at 0.15 and 1.5 μg μL^{-1}, respectively.

The effects of UPARANT on the expression and activation of VEGFR-2 were also evaluated since VEGFR-2 is known as the main mediator of VEGF effects in the retina.[53] UPARANT did not affect VEGFR-2 expression (Figs. 3A–C), while it dose-dependently reduced VEGFR-2 phosphorylation (Figs. 3A–D). In particular, VEGFR-2 phosphorylation was not affected by UPARANT at 0.0015 μg μL^{-1}, while it was reduced by approximately 32% ($P < 0.01$), 52% ($P < 0.001$), and 78% ($P < 0.001$) by UPARANT at 0.015, 0.15, and 1.5 μg μL^{-1}, respectively.

We evaluated whether UPARANT may affect HIF-1α accumulation and STAT3 phosphorylation. As shown in Figure 4, UPARANT dose-dependently reduced retinal levels of HIF-1α (Fig. 4A) and pSTAT3 (Fig. 4B). In particular, HIF-1α accumulation and STAT3 phosphorylation were not affected by UPARANT at 0.0015 and 0.015 μg μL^{-1}. On the contrary, UPARANT at 0.15 and 1.5 μg μL^{-1} reduced both HIF-1α accumulation (by approximately 50%, $P < 0.01$ and 82%, $P < 0.001$, respectively) and STAT3 phosphorylation (by approximately 49%, $P < 0.01$ and 84%, $P < 0.001$, respectively).

UPARANT Restores BRB Dysfunction

To investigate the effects of UPARANT on BRB, we measured retinal levels of occludin, a transmembrane component of interendothelial tight junctions that regulates permeability at the BRB[54] and albumin, a marker of vascular leakage.[55] In agreement with previous results,[56] OIR retinas were characterized by profound alterations in occludin and albumin levels. As shown in Figures 5A and 5B, occludin levels were lower than in controls (by approximately 76%, $P < 0.001$), but albumin levels were higher than in controls (by approximately 188%, $P < 0.001$). UPARANT at 1.5 μg μL^{-1} increased occludin while decreased albumin to levels that were not different from those in controls. Blood–retinal barrier integrity was also qualitatively evaluated by Evans blue, a dye which binds to plasma proteins. In vehicle-treated retinas, BRB breakdown was well evident as characterized by the extravasation of Evans blue bound to circulating proteins (Fig. 5C), whereas BRB breakdown was clearly reduced by UPARANT, as evidenced by the decrease of dye leakage into the retinal parenchyma (Fig. 5D).

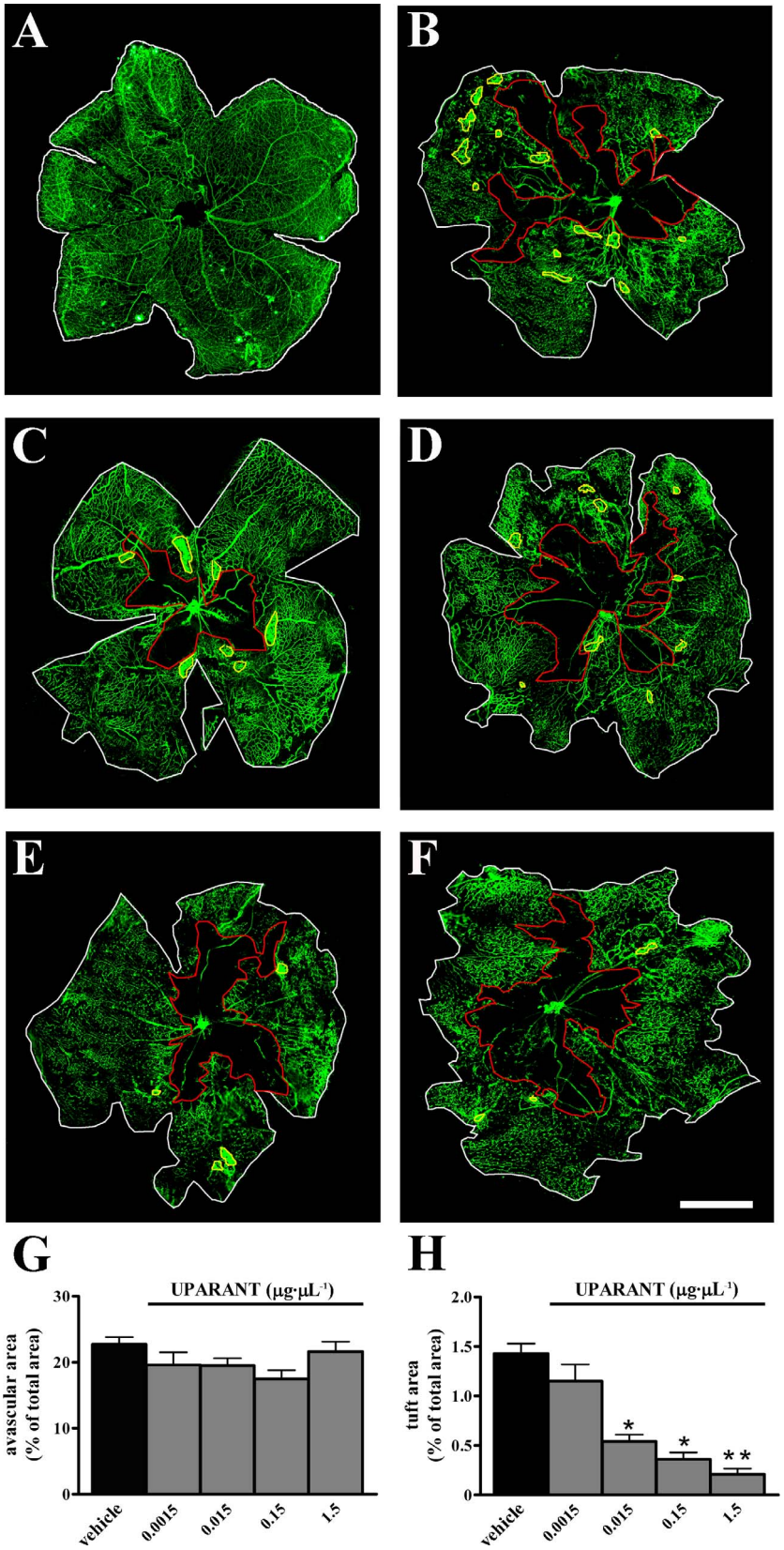

Figure 2. Flat-mounted retinas immunolabeled with a rat monoclonal antibody directed to CD31. Mice exposed to room air (**A**) or to 75% ± 2% oxygen from PD7 to PD12 (**B–F**), intravitreally injected with vehicle (PBS) in the right eye (**B**) or with UPARANT at 0.0015 (**C**), 0.015 (**D**), 0.15 (**E**), or 1.5 μg μL^{-1} (**F**) in the left eye at PD12 and PD15. Retinas were explanted at PD17. In OIR, retinas are characterized by the loss of blood vessels in the central area and the formation of neovascular tufts in the midperipheral region. *Scale bar*: 1.5 mm. The retina in (**B**) is the vehicle control of the retina in (**F**). (**G**, **H**) Quantitative analysis was performed in the entire retina. In each whole mount, the extent of the avascular area (*red contours*, [**G**]) and the total area of neovascular tufts (*yellow contours*, [**H**]) were evaluated. UPARANT did not affect the extent of the avascular area while it

dose-dependently reduced the neovascular tuft area (*$P < 0.001$ and **$P < 0.0001$ versus vehicle treated; ANOVA). Each column represents the mean ± SEM of data from six retinas.

UPARANT Recovers Dysfunctional ERG

We determined the effects of UPARANT at 1.5 μg μL^{-1} on ERG responses to light stimulation. Representative mixed a- and b-waves, and OPs recorded from control and OIR mice, vehicle or UPARANT treated, are shown in Figure 6A. In Figures 6B through 6D, the amplitude of a- and b-waves, as well as SOPs, at light intensity of 1 log cd-s.m^{-2} is reported. As previously described,[37,41,43] OIR mice displayed significantly reduced amplitude of a- and b-waves, and SOPs compared with controls. In mice with OIR, UPARANT significantly increased the amplitude of a- and b-waves, and SOPs with respect to vehicle administration. As shown in Figure 6, in control mice, neither vehicle nor UPARANT influenced ERG responses.

UPARANT Does Not Affect Retinal Structure

Oxygen-induced retinopathy is characterized by increased levels of apoptosis-related proteins leading to retinal degeneration.[57] We assessed whether increasing concentrations of UPARANT might influence the levels of proapoptotic markers, and we found that Bax/Bcl-2 ratio and cytochrome c were not affected by the drug at any concentration used (Figs. 7A, 7B), suggesting that UPARANT did not have any toxic effect on retinal cells. In concomitance with upregulation of proapoptotic markers, retinal cell loss was demonstrated by TUNEL-positive cells that were abundantly present during the ischemic phase at PD14. This apoptosis led to a significant thinning of inner plexiform and inner nuclear and outer plexiform layers at PD17, 3 days after the apoptosis occurred.[21,57,58] As shown by Figures 7C through 7E, some TUNEL-positive cells and reduced retinal thickness could be observed in OIR compared with control retinas. No appreciable differences in TUNEL staining and retinal thickness could be observed between retinas treated with vehicle and retinas treated with UPARANT at 1.5 μg μL^{-1} (Figs. 7C–F).

UPARANT Reduces the Expression of Inflammatory Markers

Inflammation is a common feature of diseases associated with retinal neovascularization and BRB dysfunction.[59] Müller cells are

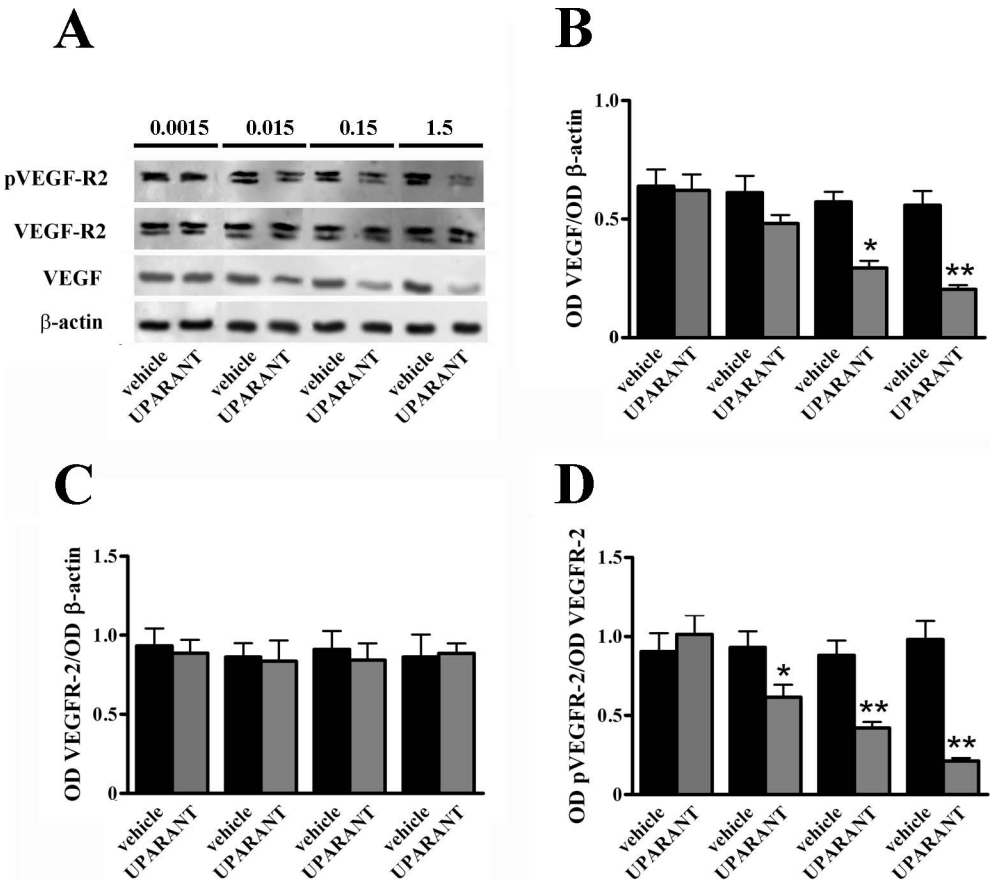

FIGURE 3. UPARANT reduces VEGF upregulation and VEGFR-2 activation. Mice were exposed to 75% ± 2% oxygen from PD7 to PD12 and intravitreally injected with vehicle (PBS) in the right eye or with UPARANT (0.0015, 0.015, 0.15, or 1.5 μg μL^{-1}) in the left eye at PD12 and PD15. Retinas were explanted at PD17, and Western blot and densitometric analysis were performed. (**A**) Representative blots depicting retinal levels of VEGF, VEGFR-2, and pVEGFR-2 after treatment with vehicle or UPARANT. (**B–D**) Densitometric analysis showing the effects of UPARANT on the expression of VEGF (**B**), VEGFR-2 (**C**), and pVEGFR-2 (**D**). The expression of both VEGF and VEGFR-2 was relative to the loading control β-actin. Expression of pVEGFR-2 was normalized to the levels of VEGFR-2. UPARANT dose-dependently reduced VEGF levels and VEGFR-2 activation while did not affect VEGFR-2 levels (*$P < 0.01$ and **$P < 0.001$ versus vehicle treated; ANOVA). Each column represents the mean ± SEM of data from five independent samples.

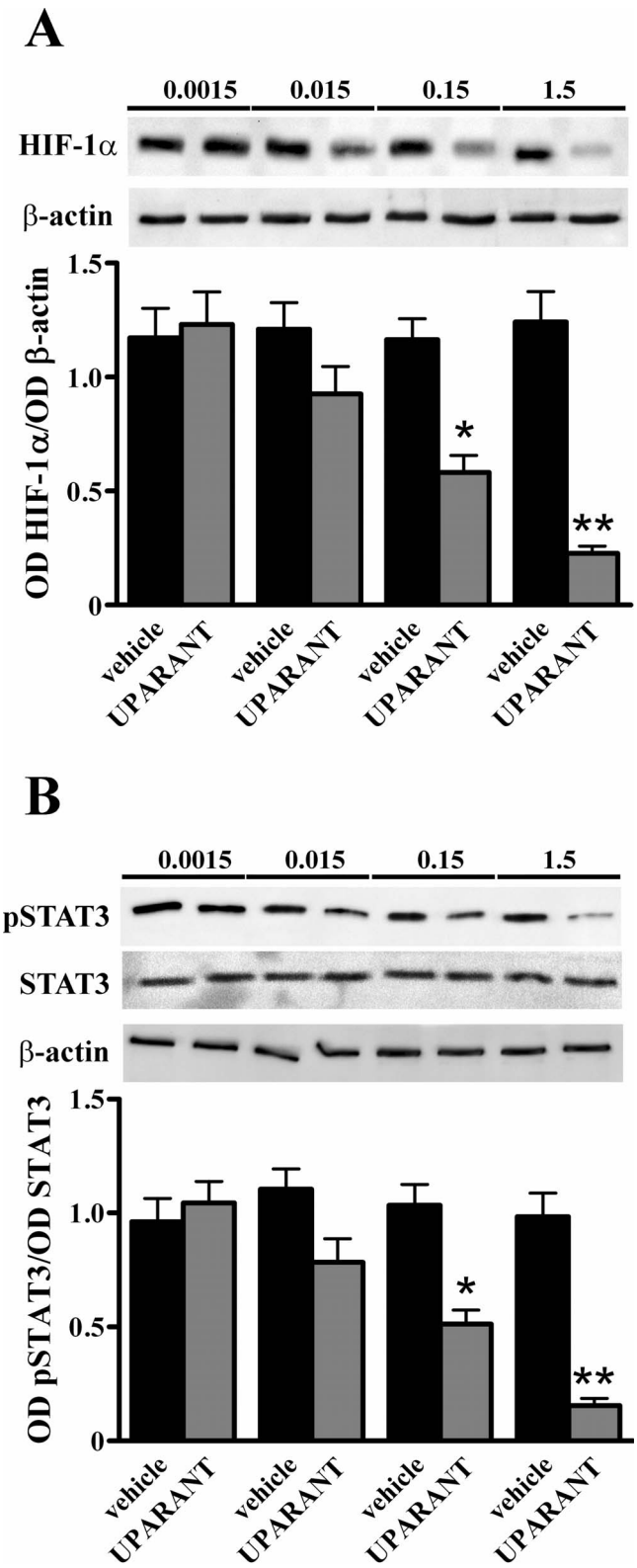

FIGURE 4. UPARANT reduces HIF-1α accumulation and STAT3 phosphorylation. Mice were exposed to 75% ± 2% oxygen from PD7 to PD12 and intravitreally injected with vehicle (PBS) in the right eye or with UPARANT (0.0015, 0.015, 0.15, or 1.5 μg μL^{-1}) in the left eye at PD12 and PD15. Retinas were explanted at PD17. (**A**) HIF-1α accumulation and (**B**) STAT3 phosphorylation as evaluated by Western blot and densitometric analysis. The expression of HIF-1α was relative to the loading control β-actin. Expression of pSTAT3 was normalized to the levels of STAT3. UPARANT dose-dependently reduced HIF-1α accumulation and STAT3 phosphorylation (*$P < 0.01$ and **$P < 0.001$ versus vehicle treated; ANOVA). Each column represents the mean ± SEM of data from five independent samples.

the principal glial cells of the retina, and in retinopathies, they become the major producer of inflammatory markers including TNF-α, IL-1β, IL-6, iNOS, ICAM-1, and GFAP.[60] We evaluated the effects of UPARANT at 1.5 μg μL^{-1} on inflammatory markers by measuring their mRNA levels. As shown in Figure 8, OIR retinas were characterized by a significant increase in the expression of inflammatory markers.[19] As shown in Figures 8A through 8F, the expression of TNF-α, IL-1β, IL-6, iNOS, ICAM-1, and GFAP mRNAs increased by approximately 256% ($P < 0.001$), 282% ($P < 0.001$), 133% ($P < 0.01$), 150% ($P < 0.05$), 263% ($P < 0.001$), and 365% ($P < 0.001$), respectively. UPARANT reduced levels of TNF-α, IL-1β, IL-6, iNOS, ICAM-1, and GFAP mRNAs by approximately 38% ($P < 0.01$), 48% ($P < 0.001$), 66% ($P < 0.01$), 50% ($P < 0.05$), 41% ($P < 0.001$), and 83% ($P < 0.001$), respectively. After UPARANT, the expression of TNF-α, IL-1β, and ICAM-1 mRNAs was higher than in controls by approximately 119% ($P < 0.05$), 98% ($P < 0.05$), and 114% ($P < 0.001$), respectively.

UPARANT Reduces the Angiogenic Activity Induced by the Vitreous Fluid From PDR Patients in Angiogenesis Assays

The evaluation of the angiogenic effects exerted by the vitreous fluid obtained after pars plana vitrectomy may provide a useful tool for a preclinical screening of angiostatic molecules with potential implications for the therapy of PDR.[29–32] Endothelial sprouts from HUVEC spheroids embedded in 3D fibrin gel and neovessel formation in chick embryo CAM represent well-established angiogenesis assays.[61] In both assays, UPARANT induces a significant inhibition of the proangiogenic activity induced by treatment with VEGF (Supplementary Fig. S1). On this basis, preliminary experiments were performed to define the amount of the vitreous fluid that exerts an optimal angiogenic response in HUVEC sprouting assay and chick embryo CAM assay. Given the limited amount of fluid available from each patient, samples obtained from 18 patients were pooled in three groups, each containing the vitreous fluids from six patients. The vitreous fluid (1:4 dilution) provided an angiogenic stimulus similar to that exerted by 30 ng mL^{-1} VEGF in HUVEC sprouting assay, while 2.0 μL vitreous fluid provided an angiogenic stimulus similar to that exerted by 0.1 μg VEGF in chick embryo CAM assay. Comparable results were obtained with the three distinct pools of vitreous fluid (data not shown). Then, we evaluated whether PDR vitreous fluid might interfere with the binding of UPARANT to endothelial cell surface with consequent UPARANT internalization. Human umbilical vein endothelial cells were incubated with 0.15 mM FITC-UPARANT in the absence or in the presence of the vitreous fluid. As shown in Supplementary Figure S2, binding and internalization of 0.15 mM FITC-UPARANT were not affected by the vitreous fluid while they were prevented by unlabeled UPARANT at 1.5 mM.

Finally, we evaluated the antiangiogenic potential of UPARANT in the presence of the vitreous fluid. UPARANT counteracted the proangiogenic activity exerted by the vitreous fluid in HUVEC (Fig. 9A) and chick embryo CAM (Fig. 9B) sprouting assays. In particular, in HUVEC assay, sprouts were reduced by approximately 36% ($P < 0.05$), 41% ($P < 0.05$), 72% ($P < 0.001$), and 68% ($P < 0.001$) by UPARANT at 0.001, 0.01, 0.1, and 1 nM, respectively, while in chick embryo CAM assay, the number of vessels was reduced by approximately 24% ($P < 0.01$), 50% ($P < 0.001$), and 61% ($P < 0.001$) by UPARANT at 0.01, 0.1, and 1 μg, respectively.

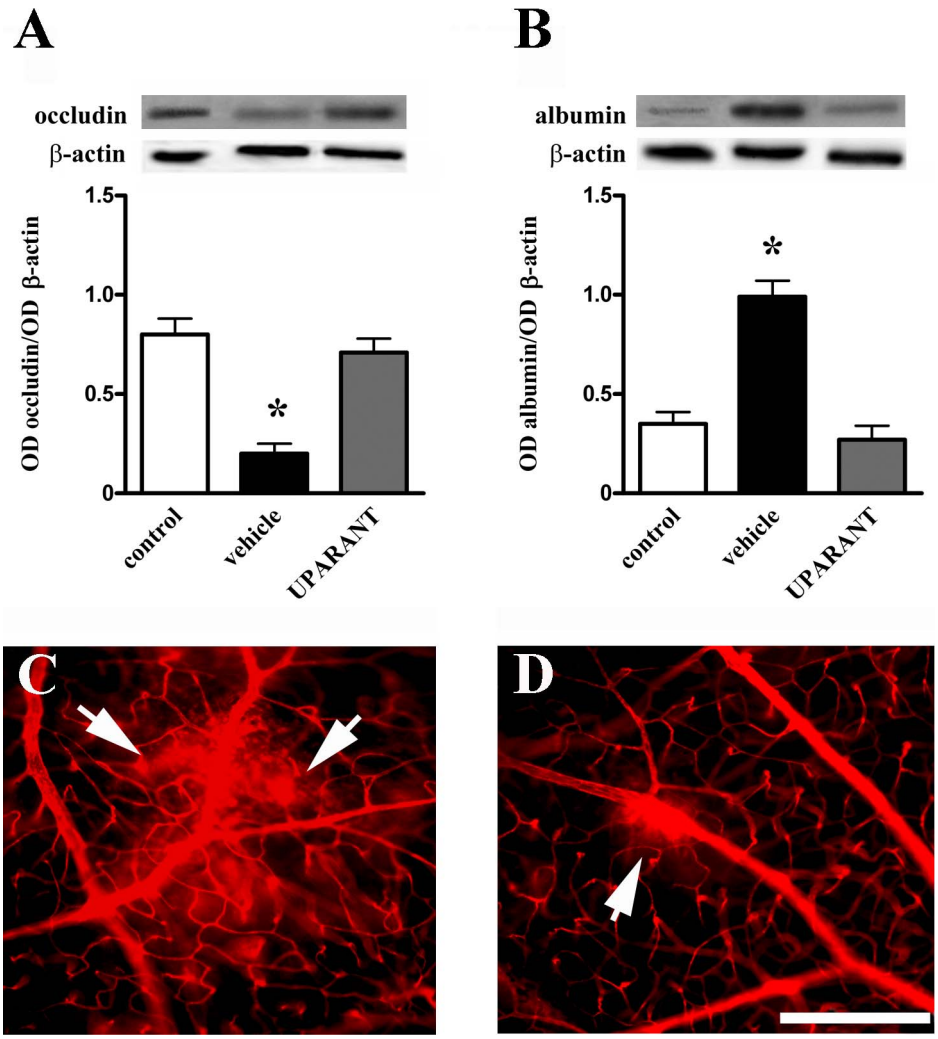

Figure 5. UPARANT reduces BRB breakdown. Mice were exposed to room air (control) or to 75% ± 2% oxygen from PD7 to PD12. Oxygen-induced retinopathy mice were intravitreally injected with vehicle (PBS) in the right eye or with 1.5 μg μL^{-1} UPARANT in the left eye at PD12 and PD15. Retinas were explanted at PD17. (**A**) Levels of occludin and (**B**) albumin in control, vehicle- or UPARANT-treated retinas, as evaluated by Western blot and densitometric analysis. The expression of proteins was relative to the loading control β-actin. UPARANT prevented the decrease in occludin and the increase in albumin levels (*$P < 0.001$ versus control; ANOVA). Each column represents the mean ± SEM of data from five independent samples. (**C**, **D**) Blood–retinal vascular leakage as qualitatively evaluated with the Evans blue method in vehicle- (**C**) and in UPARANT- (**D**) treated retinas. *Arrows*: Vascular leakage. Six mice were used for each experimental condition. *Scale bar*: 200 μm.

Discussion

There is a strong need of new drugs specifically targeting angiogenesis-associated retinal diseases with minimal side effects. The uPA/uPAR system is a promising target for the development of antiangiogenic drugs as in the retina, ischemia/hypoxia is known to activate this system, which contributes to promoting angiogenesis.[8] In general, compared with anti-VEGF antibodies or VEGF decoy soluble receptors, oligopeptides such as UPARANT show several advantages including higher activity per unit mass, greater stability, reduced interactions with the immune system, and better penetration.[62] The present data demonstrate for the first time that UPARANT is effective against retinal angiogenesis in response to ischemia. The additional fact that UPARANT counteracts the angiogenic potential of PDR vitreous fluid confers an extra value to the potential application of UPARANT. Whether further investigations will clarify the mechanism of action of UPARANT, then this drug may open the field for the development of novel therapeutic approaches to counteract pathologic neovascularization in the retina.

UPARANT Acts at Different Concentrations In Vitro, Ex Vivo, and In Vivo

In the ex vivo murine retinal angiogenesis assay and the HUVEC sprouting assay, UPARANT was used at concentrations ranging from 1 pM to 1 nM in agreement with previous observations on UPARANT capacity to inhibit VEGF-induced angiogenesis in HUVECs.[13] Higher concentrations of UPARANT were used in OIR mice. In fact, UPARANT was injected intravitreally at doses ranging from 0.0015 to 1.5 μg μL^{-1} that correspond to molar concentrations ranging from 0.45 μM to 0.45 mM when considering a vitreous volume of approximately 5.3 μL. Similarly, UPARANT was delivered onto the chick embryo CAM at doses ranging between 0.01 and 1 μg $implant^{-1}$.

Differences in terms of the pharmacokinetic profile of the drug may explain its apparent different potency in the in vitro

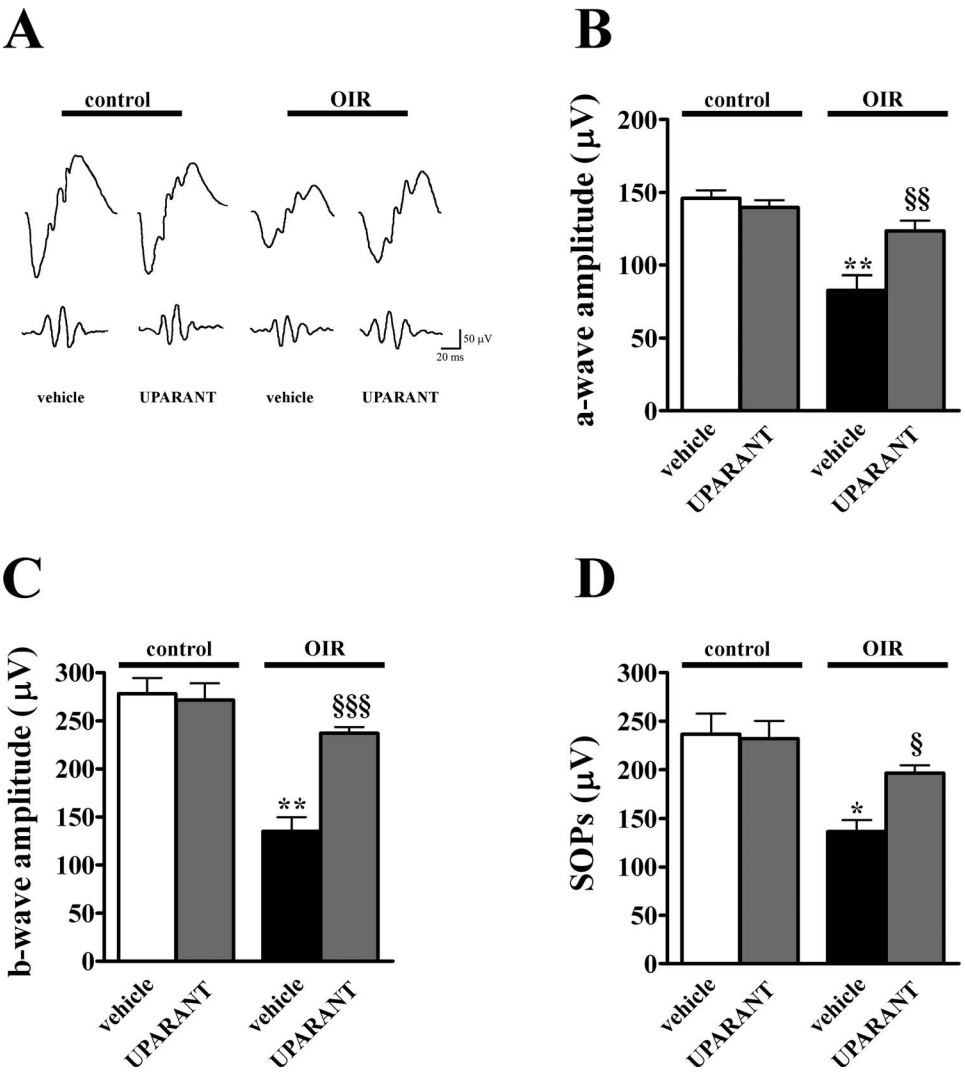

Figure 6. UPARANT restores ERG responses. Mice were exposed to room air (control) or to 75% ± 2% oxygen from PD7 to PD12 and were intravitreally injected in both eyes with vehicle (PBS) or with 1.5 µg μL^{-1} UPARANT at PD12 and PD15. Electroretinogram was recorded at PD17. (**A**) Representative ERG waveforms (*top*) and OPs (*bottom*) in control and OIR mice treated with vehicle or UPARANT recorded at light intensity of 1 log cd-s.m^{-2}. (**B–D**) a-wave amplitudes (**B**), b-wave amplitudes (**C**), and SOPs (**D**) in control and OIR mice treated with vehicle or UPARANT at light intensity of 1 log cd-s.m^{-2}. UPARANT restored a-wave, b-wave, and SOPs (*$P < 0.01$ and **$P < 0.001$ versus control, §$P < 0.05$, §§$P < 0.01$, and §§§$P < 0.001$ versus vehicle treated; ANOVA). Each column represents the mean ± SEM of data from six mice for each experimental condition.

versus the in vivo assays. Indeed, UPARANT added to the medium can interact directly with endothelial cells in culture, whereas its delivery into the posterior eye chamber requires the molecule to diffuse through the vitreous in order to reach the retina. In addition, the half-life in the vitreous is another factor that can determine the efficacy of the drug. In fact, following intraocular injection, the actual vitreal concentration of UPARANT can be substantially lowered by elimination routes through the aqueous humor in the anterior chamber or the BRB in the posterior chamber.[63] There are several reports of drugs tested at higher concentrations when injected into the posterior chamber of the eye than those used in in vitro models—for example, endostatin tested for its antiangiogenic properties at 70 µM when intraocularly injected but at 5 nM in HUVECs.[64] Analogously, higher concentrations of UPARANT are needed to diffuse out the alginate plug and through the embryonic epithelium to interact with mesenchymal CAM vessels. Additionally, differences in timing of the various assays and in the stability of the molecule may affect the potency of UPARANT in the different experimental conditions.

Effects of UPARANT on Retinal Angiogenesis

In agreement with previous results demonstrating antiangiogenic properties of UPARANT,[13] the present results demonstrate that UPARANT is highly effective in inhibiting VEGF-driven angiogenesis by preventing the formation of vessel sprouts in a murine assay of retinal angiogenesis as well as in HUVEC sprouting and chick embryo CAM neovessel growth. This finding provides evidence that VEGF-induced vessel sprouting is dependent on the activation of uPAR. In this line, the activation of the uPA/uPAR system represents an essential regulatory mechanism in endothelial cell migration induced by growth factors, including VEGF.[65]

As also shown by the present results, in OIR mice, UPARANT ameliorates retinal angiogenesis by reducing neovascular tuft formation in the midperipheral retina without affecting the central avascular area. This finding demonstrates for the first time that UPARANT is effective in counteracting angiogenesis in an in vivo model and confirms the role of the uPA/uPAR system in regulating retinal neovascularization.[8,66]

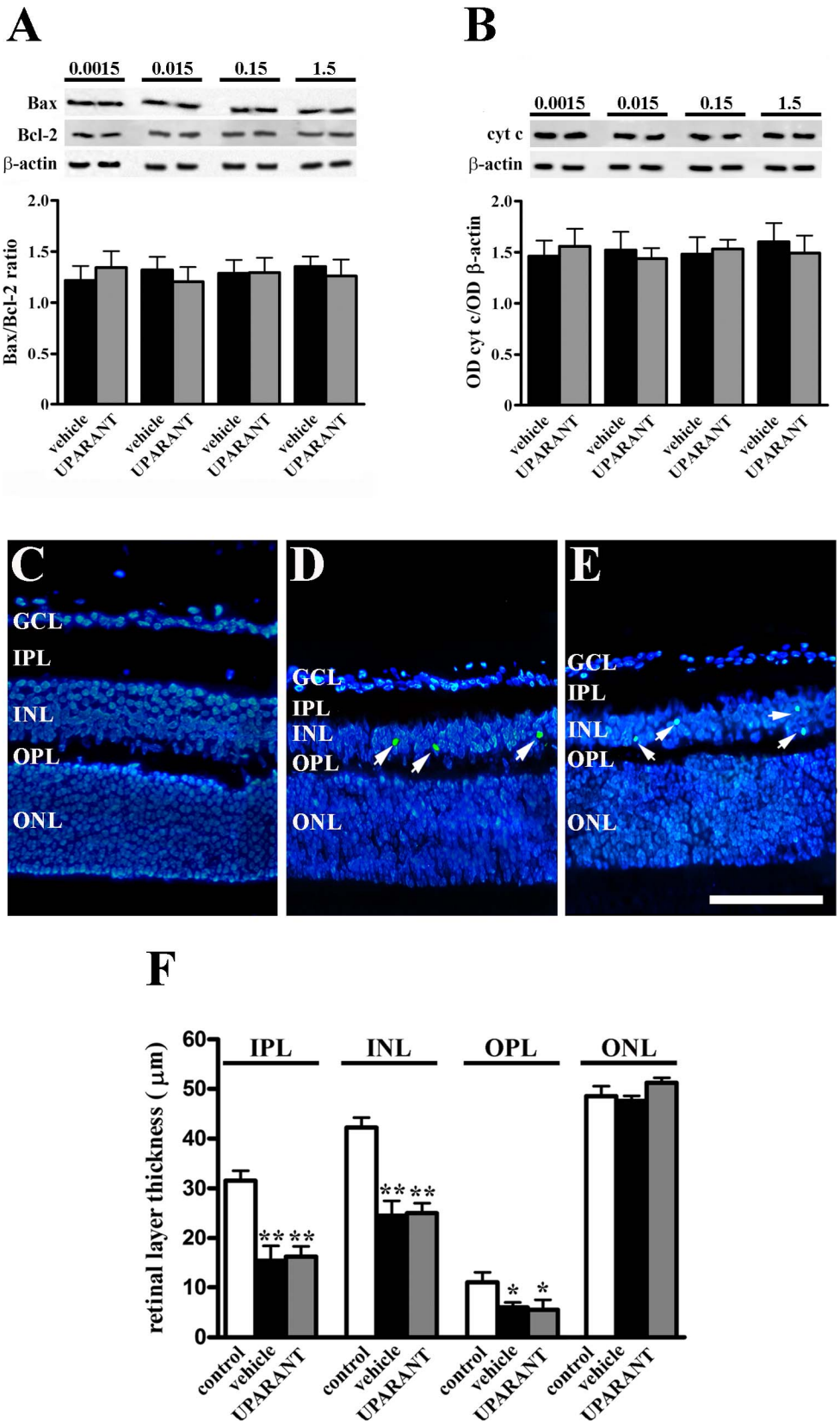

Figure 7. UPARANT does not influence retinal cell apoptosis and retinal cytoarchitecture. (**A**, **B**) Mice were exposed to 75% ± 2% oxygen from PD7 to PD12 and intravitreally injected with vehicle (PBS) in the right eye or with UPARANT (0.0015, 0.015, 0.15, or 1.5 μg μL^{-1}) in the left eye at PD12 and PD15. Retinas were explanted at PD17, and Western blot and densitometric analysis were performed to evaluate Bax/Bcl-2 ratio (**A**) or cytochrome c levels (**B**). The expression of Bax was normalized to the levels of Bcl-2. The expression of cytochrome c was relative to the loading control β-actin. UPARANT does not affect Bax/Bcl-2 ratio or cytochrome c levels. Each column represents the mean ± SEM of data from five independent samples. (**C**–**E**) Retinal sections from mice exposed to room air (control, [**C**]) and from OIR mice treated with vehicle (**D**) or 1.5 μg μL^{-1}

UPARANT (**E**) killed at PD17. Sections were stained by TUNEL (*green*) and DAPI (*blue*). Representative images are shown. TUNEL-positive cells are indicated by *arrows*. UPARANT did not affect the number of TUNEL-positive retinal cells. (**F**) The thickness of retinal layers was evaluated. UPARANT did not affect retinal thickness (*$P < 0.05$ and **$P < 0.01$ versus control; ANOVA). Each column represents the mean ± SEM of data from five retinas. GCL, ganglion cell layer; IPL, inner plexiform layer; INL, inner nuclear layer; OPL, outer plexiform layer; ONL, outer nuclear layer. *Scale bar*: 50 μm.

In line with the present data, inhibition of the uPA/uPAR system reduces choroidal neovascularization in a mouse model of AMD, suggesting that UPARANT may be potentially therapeutic for several types of ocular diseases characterized by pathologic angiogenesis.[12]

The finding that UPARANT inhibits the formation of neovascular tufts without affecting the avascular area suggests that the uPA/uPAR system is important for the development of neovascular tufts, having only a minor role, if any, in the revascularization of the central avascular area. In this respect, in OIR retinas, uPAR is upregulated in endothelial cells of the superficial vascular plexus, in particular, in cells lining neovascular tufts.[8] On the other hand, the lack of effects of UPARANT on the avascular area can also be explained by the fact that UPARANT administration begins at PD12 when the avascular area is already formed.

As shown by the present results, UPARANT reduces the levels of VEGF indicating that uPAR activation may regulate VEGF expression and suggesting a causal relationship between the effects of UPARANT on VEGF and the amelioration of pathologic neovascularization. In line with this hypothesis, uPAR inhibition or *uPAR* gene deletion results in decreased VEGF expression in some tumor models.[14–16]

Consistent with UPARANT-induced downregulation of VEGF, the present findings also demonstrate a reduced activation of VEGFR-2, the receptor that principally mediates the proangiogenic action of VEGF,[53] thus providing the first demonstration that uPAR is coupled to a modulation of the VEGF system in response to ischemic conditions. There are indications that reduced activation of VEGFR-2 is a consequence of VEGF downregulation (e.g., in the rat retina).[67] On the other hand, the possibility that UPARANT affects VEGFR-2 activity independently on its effects on VEGF cannot be excluded since uPAR is known to directly activate VEGFR-2 in either HUVECs or human dermal endothelial cells.[68] The additional fact that UPARANT reduces the expression of HIF-1α and pSTAT3, which are two key regulators of VEGF expression,[69,70] suggests that the drug may act as a modulator of the VEGF/VEGFR-2 axis. UPARANT action described here is consistent with data in glioma cells reporting that uPAR silencing downregulates VEGF expression by reducing the activity of both HIF-1 and STAT3.[14] It has been shown that in

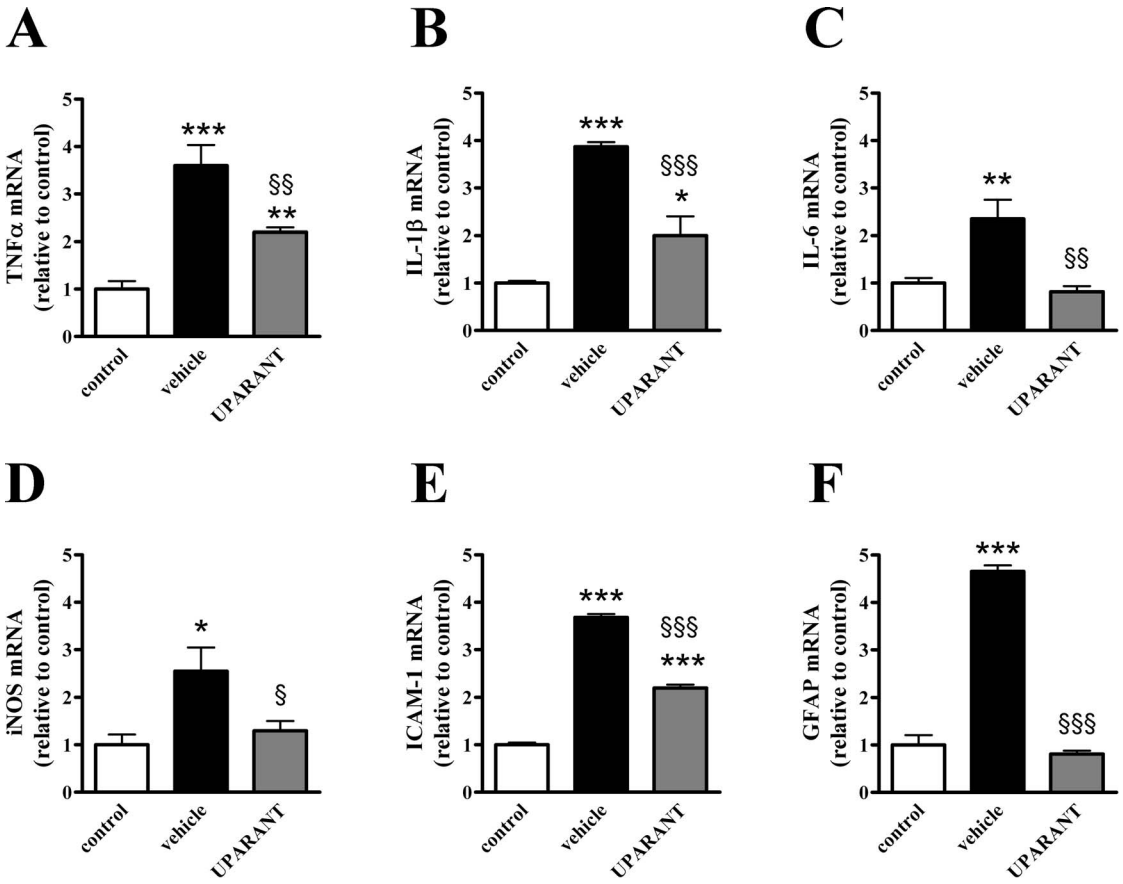

Figure 8. UPARANT reduces levels of inflammatory markers. Mice were exposed to room air (control) or to 75% ± 2% oxygen from PD7 to PD12. OIR mice were intravitreally injected with vehicle (PBS) in the right eye or with 1.5 μg μL^{-1} UPARANT in the left eye at PD12 and PD15. Retinas were explanted at PD17. Levels of mRNA of TNF-α (**A**), IL-1β (**B**), IL-6 (**C**), iNOS (**D**), ICAM-1 (**E**), and GFAP (**F**) were evaluated by QPCR. Data were analyzed by the formula $2^{-\Delta\Delta CT}$ using Rpl13a as internal standard. UPARANT reduced mRNA levels of inflammatory markers (*$P < 0.05$, **$P < 0.01$, and ***$P < 0.001$ versus control; §$P < 0.05$, §§$P < 0.01$, and §§§$P < 0.001$ versus vehicle treated; ANOVA). Each column represents the mean ± SEM of data from five independent samples.

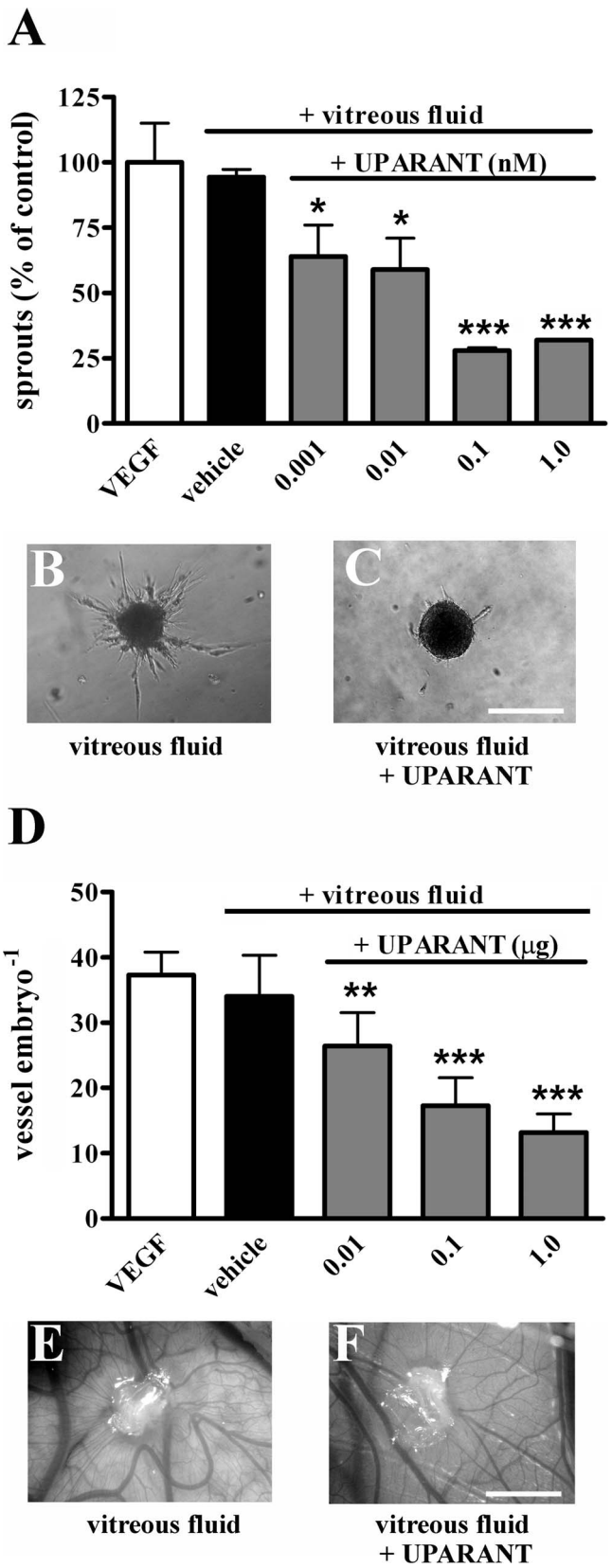

Figure 9. UPARANT inhibits the angiogenic activity of the vitreous fluid from PDR patients. (**A**) HUVEC spheroids embedded in fibrin gel were incubated in the presence of either VEGF (30 ng mL^{-1}) or PDR vitreous fluid in combination with vehicle (PBS) or increasing concentrations of UPARANT. After 24 hours, vessel sprouts were counted. (**B**, **C**) Representative images of HUVEC spheroids treated with PDR vitreous fluid in the presence of either vehicle or 0.1 nM UPARANT. (**D**) Chick embryo CAMs were implanted at day 11 after fertilization with alginate beads containing either 0.1 μg VEGF or 2.0 μL PDR vitreous fluid in combination with vehicle (PBS) or increasing amounts of UPARANT. After 3 days, newly formed blood vessels converging versus the implant were counted. (**E**, **F**) Representative images of chick embryo CAMs treated with PDR vitreous fluid in the presence of either vehicle or 0.1 μg UPARANT. UPARANT dose-dependently reduced angiogenesis in both the assays (*$P < 0.05$, **$P < 0.01$, and ***$P < 0.001$ versus vehicle treated; ANOVA). Each column represents the mean ± SEM of data from 30 HUVEC spheroids or eight implanted eggs. *Scale bars*: 150 μm (**C**) or 5 mm (**F**).

several assays, UPARANT counteracts VEGF-induced angiogenesis by preventing the activation of FPRs and integrins.[13] In addition, it has been reported that integrins may activate STAT3 signaling in tumor cells.[71] Although more work remains to be done in order to clarify the mechanism of action of UPARANT, the possibility exists that this drug may modulate the activity of transcription factors by blocking the activation of integrins.

Effects of UPARANT on BRB

We have shown that UPARANT reduces the leakage from vessels as it restores the tight junction protein occludin and decreases albumin extravasation. The fact that UPARANT counteracts BRB breakdown is in line with the finding that upregulation of the uPA/uPAR system is a main cause of vascular leakage as demonstrated in DR.[11,72,73] The possibility exists that UPARANT-induced reduction of VEGF levels may be responsible for the amelioration of vascular leakage. In fact, VEGF plays an important role as a permeable factor inducing alterations of tight junction proteins, which result in BRB breakdown.[20] On the other hand, we cannot exclude the possibility that a VEGF-independent mechanism may mediate, at least in part, UPARANT-induced amelioration of BRB breakdown as the uPA/uPAR system has been shown to directly activate proteases that promote BRB breakdown in DR.[11,72]

Effects of UPARANT on Visual Function

Pathologic neovascularization, retinal degeneration, and glial activation are the main mechanisms involved in OIR models.[74] Apoptosis plays a pivotal role in retinal degeneration with apoptotic cells mainly located in the inner nuclear layer,[57] although rod dysfunction has been also reported to precede vascular abnormalities and to predict the subsequent alterations of the vascular status.[75]

The alterations in retinal structure may result in profound retinal dysfunction,[43] and there is evidence that ameliorating angiogenesis may also be effective in preventing visual loss.[37,41,76] However, treatments that counteract pathologic neovascularization may not necessarily prevent retinal dysfunction.[77]

As shown by the present results, inhibiting uPAR signaling is effective in recovering dysfunctional ERG without influencing retinal cell apoptosis and the gross morphology of the retina. This finding suggests that ERG recovery from visual loss does not necessarily involve protection from apoptosis. For instance, omega-3 polyunsaturated fatty acids preserve retinal function without exerting cytoprotective effects in the retina of diabetic mice.[21] Additionally, ERG alterations are not necessarily a consequence of retinal cell death, but rather of glial activation and inflammation. For instance, in DR, ERG alterations occur in concomitance with microglial reaction but without neural cell death.[78] In this respect, Müller cells—

which are the main source of inflammatory markers in retinopathies[79]—are believed to generate several components of the ERG.[80] The fact that UPARANT restores OIR-induced upregulation of inflammatory markers suggests that its protective effects on retinal function may depend on reducing inflammation. In line with this possibility, inhibition of inflammatory cytokines by anti-inflammatory drugs prevents ERG dysfunction in a model of retinal ischemia.[81]

As irreversible visual loss represents one of the most important clinical problems of proliferative retinopathies and its prevention/recovery is limited by the scarce availability of drugs restoring visual function, the fact that UPARANT, possibly as a consequence of vascular rescue and ameliorated inflammation, recovers ERG adds further relevance to its potential application and confirms the close relationship between vascular damages and neural dysfunction in the pathophysiology of proliferative retinopathies.[82]

Effects of UPARANT on Angiogenesis Induced by PDR Vitreous Fluid

The finding that PDR vitreous fluid does not affect the binding of UPARANT to endothelial cell surface and consequent UPARANT internalization indicates that the vitreous fluid does not contain molecules possibly interfering with the binding of UPARANT to uPAR. As also shown by the present results, the vitreous fluid elicits a potent angiogenic response in line with previous findings.[29–32] Vascular endothelial growth factor is a major stimulator of retinal neovascularization in PDR although other growth factors likely play an important role as well. Therefore, the overall angiogenic potential of the vitreous fluid may represent the result of the synergistic action of various angiogenic factors. In fact, the amount of VEGF (i.e., 30 ng mL^{-1} in HUVEC sprouting assay and 0.1 μg in chick embryo CAM assay) required to induce an angiogenic response similar to that exerted by the vitreous fluid far exceeds the concentration of VEGF detectable in the vitreous fluid (median VEGF levels equal to 345 pg mL^{-1} as reported by Watanabe et al.[31]). In this line, in the rat, intravitreal injection of PDR vitreous fluid determines an increase in BRB leakage, which is higher than that induced by intravitreal injection of VEGF.[83] For this reason, a more complete antiangiogenic effect in retinopathies will likely require the ability to block multiple growth factors. In this respect, the fact that UPARANT is effective in counteracting angiogenic processes elicited by PDR vitreous fluid indicates that UPARANT not only prevents VEGF-induced angiogenesis, but it may also block the angiogenic potential of additional proangiogenic factors contained in the vitreous fluid. Consistently, it has been observed that interfering with the uPA/uPAR system reduces the migratory response of endothelial cells induced not only by VEGF, but also by fibroblast growth factor 2, epidermal growth factor, and hepatocyte growth factor.[65]

These preliminary data obtained in angiogenic assays cannot be immediately extrapolated to the in vivo situation. To evaluate the translational impact of the present findings, further studies in animal models will be necessary.

Conclusions

The search for effective treatments for retinal neovascular disorders remains one of the greatest challenges in ophthalmology. Current anti-VEGF therapies used in the treatment of proliferative ocular diseases may have relatively limited efficacy. In this respect, UPARANT, a stable uPAR inhibitor, may represent a significant step forward in the development of new antiangiogenic strategies. Indeed, the present data show that UPARANT is effective against retinal neovascularization and that suppresses the angiogenic potential of PDR vitreous fluid indicating a potential advantage over classical anti-VEGF drugs. Although extrapolation of these experimental findings to the human situation is difficult, UPARANT has potential as a new therapeutic strategy for proliferative retinopathies.

Acknowledgments

The authors thank Vincenzo Pavone for providing UPARANT and FITC-UPARANT. The authors also thank Irene Fornaciari for technical assistance in immunohistochemistry and Gino Bertolini for the assistance in animal care.

Supported by grants from Regione Toscana (NOVASA project, PB; Florence, Italy); Ministero dell'Istruzione, Università e Ricerca (FIRB Grant n° RBAP11H2R9, MP; Rome, Italy); Associazione Italiana per la Ricerca sul Cancro (AIRC Grant n° 14395, MP; Milan, Italy); and Bioos Italia (PB and MP; Montegiorgio, Italy).

Disclosure: **M. Dal Monte**, None; **S. Rezzola**, None; **M. Cammalleri**, None; **M. Belleri**, None; **F. Locri**, None; **L. Morbidelli**, None; **M. Corsini**, None; **G. Paganini**, None; **F. Semeraro**, None; **A. Cancarini**, None; **D. Rusciano**, None; **M. Presta**, None; **P. Bagnoli**, None

References

1. Montuori N, Ragno P. Role of uPA/uPAR in the modulation of angiogenesis. *Chem Immunol Allergy*. 2014;99:105–122.
2. Uhrin P, Breuss JM. uPAR: a modulator of VEGF-induced angiogenesis. *Cell Adh Migr*. 2013;7:23–26.
3. Binder BR, Mihaly J, Prager GW. uPAR-uPA-PAI-1 interactions and signaling: a vascular biologist's view. *Thromb Haemost*. 2007;97:336–342.
4. Bifulco K, Longanesi-Cattani I, Gala M, et al. The soluble form of urokinase receptor promotes angiogenesis through its Ser88-Arg-Ser-Arg-Tyr92 chemotactic sequence. *J Thromb Haemost*. 2010;8:2789–2799.
5. Ramsey DJ, Haddock LJ, Young LH, Eliott D. Complications of subspecialty ophthalmic care: systemic complications from the intravitreal administration of agents that target the vascular endothelial growth factor pathway. *Semin Ophthalmol*. 2014; 29:263–275.
6. Fleck BW. Management of retinopathy of prematurity. *Arch Dis Child Fetal Neonatal Ed*. 2013;98:F454–F456.
7. Bradley J, Ju M, Robinson GS. Combination therapy for the treatment of ocular neovascularization. *Angiogenesis*. 2007; 10:141–148.
8. McGuire PG, Jones TR, Talarico N, Warren E, Das A. The urokinase/urokinase receptor system in retinal neovascularization: inhibition by A6 suggests a new therapeutic target. *Invest Ophthalmol Vis Sci*. 2003;44:2736–2742.
9. Colombo ES, Menicucci G, McGuire PG, Das A. Hepatocyte growth factor/scatter factor promotes retinal angiogenesis through increased urokinase expression. *Invest Ophthalmol Vis Sci*. 2007;48:1793–1800.
10. Sugioka K, Kodama A, Okada K, et al. TGF-β2 promotes RPE cell invasion into a collagen gel by mediating urokinase-type plasminogen activator (uPA) expression. *Exp Eye Res*. 2013; 115:13–21.
11. Navaratna D, Menicucci G, Maestas J, Srinivasan R, McGuire P, Das A. A peptide inhibitor of the urokinase/urokinase receptor system inhibits alteration of the blood-retinal barrier in diabetes. *FASEB J*. 2008;22:3310–3317.
12. Das A, Boyd N, Jones TR, Talarico N, McGuire PG. Inhibition of choroidal neovascularization by a peptide inhibitor of the

urokinase plasminogen activator and receptor system in a mouse model. *Arch Ophthalmol*. 2004;122:1844–1849.

13. Carriero MV, Bifulco K, Minopoli M, et al. UPARANT: a urokinase receptor-derived peptide inhibitor of VEGF-driven angiogenesis with enhanced stability and in vitro and in vivo potency. *Mol Cancer Ther*. 2014;13:1092–1104.
14. Malla RR, Gopinath S, Gondi CS, et al. Cathepsin B and uPAR knockdown inhibits tumor-induced angiogenesis by modulating VEGF expression in glioma. *Cancer Gene Ther*. 2011;18: 419–434.
15. Ahmad A, Kong D, Sarkar SH, Wang Z, Banerjee S, Sarkar FH. Inactivation of uPA and its receptor uPAR by 3,3′-diindolylmethane (DIM) leads to the inhibition of prostate cancer cell growth and migration. *J Cell Biochem*. 2009;107:516–527.
16. Nalabothula N, Lakka SS, Dinh DH, Guirati M, Olivero WC, Rao JS. Sense p16 and antisense uPAR bicistronic construct inhibits angiogenesis and induces glioma cell death. *Int J Oncol*. 2007; 30:669–678.
17. Grossniklaus HE, Kang SJ, Berglin L. Animal models of choroidal and retinal neovascularization. *Prog Retin Eye Res*. 2010;29:500–519.
18. Stahl A, Connor KM, Sapieha P, et al. The mouse retina as an angiogenesis model. *Invest Ophthalmol Vis Sci*. 2010;51: 2813–2826.
19. Scott A, Fruttiger M. Oxygen-induced retinopathy: a model for vascular pathology in the retina. *Eye (Lond)*. 2010;24:416–421.
20. Kaur C, Foulds WS, Ling EA. Blood-retinal barrier in hypoxic ischaemic conditions: basic concepts, clinical features and management. *Prog Retin Eye Res*. 2008;27:622–647.
21. Sapieha P, Chen J, Stahl A, et al. Omega-3 polyunsaturated fatty acids preserve retinal function in type 2 diabetic mice. *Nutr Diabetes*. 2012;2:e36.
22. Stahl A, Chen J, Sapieha P, et al. Postnatal weight gain modifies severity and functional outcome of oxygen-induced proliferative retinopathy. *Am J Pathol*. 2010;177:2715–2723.
23. Fulton AB, Hansen RM, Moskowitz A, Akula JD. The neurovascular retina in retinopathy of prematurity. *Prog Retin Eye Res*. 2009;28:452–482.
24. Fulton AB, Akula JD, Mocko JA, et al. Retinal degenerative and hypoxic ischemic disease. *Doc Ophthalmol*. 2009;118:55–61.
25. Rezzola S, Belleri M, Ribatti D, Costagliola C, Presta M, Semeraro F. A novel ex vivo murine retina angiogenesis (EMRA) assay. *Exp Eye Res*. 2013;112:51–56.
26. Shirasawa M, Arimura N, Otsuka H, Sonoda S, Hashiguchi T, Sakamoto T. Intravitreous VEGF-A in eyes with massive vitreous hemorrhage. *Graefes Arch Clin Exp Ophthalmol*. 2011;249:1805–1810.
27. Merlak M, Kovacević D, Balog T, et al. Expression of vascular endothelial growth factor in proliferative diabetic retinopathy. *Coll Antropol*. 2008;32(suppl 2):39–43.
28. Simó R, Carrasco E, García-Ramírez M, Hernández C. Angiogenic and antiangiogenic factors in proliferative diabetic retinopathy. *Curr Diabetes Rev*. 2006;2:71–98.
29. Yang J, Klassen H, Pries M, Wang W, Nissen MH. Vitreous humor and albumin augment the proliferation of cultured retinal precursor cells. *J Neurosci Res*. 2009;87:495–502.
30. Takagi H, Watanabe D, Suzuma K, et al. Novel role of erythropoietin in proliferative diabetic retinopathy. *Diabetes Res Clin Pract*. 2007;77(suppl 1):S62–S64.
31. Watanabe D, Suzuma K, Matsui S, et al. Erythropoietin as a retinal angiogenic factor in proliferative diabetic retinopathy. *N Engl J Med*. 2005;353:782–792.
32. Aiello LP, Avery RL, Arrigg PG, et al. Vascular endothelial growth factor in ocular fluid of patients with diabetic retinopathy and other retinal disorders. *N Engl J Med*. 1994; 331:1480–1487.
33. Smith LE, Wesolowski E, McLellan A, et al. Oxygen-induced retinopathy in the mouse. *Invest Ophthalmol Vis Sci*. 1994;35: 101–111.
34. Favaloro EJ, Moraitis N, Koutts J, Exner T, Bradstock KF. Endothelial cells and normal circulating haemopoietic cells share a number of surface antigens. *Thromb Haemost*. 1989; 61:217–224.
35. Dal Monte M, Casini G, la Marca G, Isacchi B, Filippi L, Bagnoli P. Eye drop propranolol administration promotes the recovery of oxygen-induced retinopathy in mice. *Exp Eye Res*. 2013; 111:27–35.
36. Dal Monte M, Martini D, Latina V, Pavan B, Filippi L, Bagnoli P. Beta-adrenoreceptor agonism influences retinal responses to hypoxia in a model of retinopathy of prematurity. *Invest Ophthalmol Vis Sci*. 2012;53:2181–2192.
37. Martini D, Dal Monte M, Ristori C, et al. Antiangiogenic effects of β(2)-adrenergic receptor blockade in a mouse model of oxygen-induced retinopathy. *J Neurochem*. 2011;119:1317–1329.
38. Banin E, Dorrell MI, Aguilar E, et al. T2-TrpRS inhibits preretinal neovascularization and enhances physiological vascular regrowth in OIR as assessed by a new method of quantification. *Invest Ophthalmol Vis Sci*. 2006;47:2125–2134.
39. Berkowitz BA, Roberts R, Luan H, Peysakhov J, Mao X, Thomas KA. Dynamic contrast-enhanced MRI measurements of passive permeability through blood retinal barrier in diabetic rats. *Invest Ophthalmol Vis Sci*. 2004;45:2391–2398.
40. Trichonas G, Manola A, Morizane Y, et al. A novel nonradioactive method to evaluate vascular barrier breakdown and leakage. *Invest Ophthalmol Vis Sci*. 2010;51:1677–1682.
41. Dal Monte M, Latina V, Cupisti E, Bagnoli P. Protective role of somatostatin receptor 2 against retinal degeneration in response to hypoxia. *Naunyn Schmiedebergs Arch Pharmacol*. 2012;385:481–494.
42. Robson JG, Saszik SM, Ahmed J, Frishman LJ. Rod and cone contributions to the a-wave of the electroretinogram of the macaque. *J Physiol*. 2003;547:509–530.
43. Vessey KA, Wilkinson-Berka JL, Fletcher EL. Characterization of retinal function and glial cell response in a mouse model of oxygen induced retinopathy. *J Comp Neurol*. 2011;519:506–527.
44. Bresnick GH, Palta M. Oscillatory potential amplitudes. Relation to severity of diabetic retinopathy. *Arch Ophthalmol*. 1987;105:929–933.
45. Hombrebueno JR, Luo C, Guo L, Chen M, Xu H. Intravitreal injection of normal saline induces retinal degeneration in the C57BL/6J mouse. *Transl Vis Sci Technol*. 2014;3(2):3.
46. Elsherbiny NM, Ahmad S, Naime M, et al. ABT-702, an adenosine kinase inhibitor, attenuates inflammation in diabetic retinopathy. *Life Sci*. 2013;93:78–88.
47. Wang X, Seed BA. PCR primer bank for quantitative gene expression analysis. *Nucleic Acids Res*. 2003;31:e154.
48. Pattyn F, Speleman F, De Paepe A, Vandesompele J. RTPrimerDB: the real-time PCR primer and probe database. *Nucleic Acids Res*. 2003;31:122–123.
49. Mazumder B, Sampath P, Seshadri V, Maitra RK, DiCorleto PE, Fox PL. Regulated release of L13a from the 60S ribosomal subunit as a mechanism of transcript-specific translational control. *Cell*. 2003;115:187–198.
50. Livak KJ, Schmittgen TD. Analysis of relative gene expression data using real-time quantitative PCR and the 2(–Delta Delta C(T)) method. *Methods*. 2001;25:402–408.
51. Stabile H, Mitola S, Moroni E, et al. Bone morphogenic protein antagonist Drm/gremlin is a novel proangiogenic factor. *Blood*. 2007;109:1834–1840.
52. Mitola S, Moroni E, Ravelli C, Andres G, Belleri M, Presta M. Angiopoietin-1 mediates the proangiogenic activity of the

bone morphogenic protein antagonist Drm. *Blood*. 2008;112: 1154–1157.

53. Olsson AK, Dimberg A, Kreuger J, Claesson-Welsh L. VEGF receptor signalling - in control of vascular function. *Nat Rev Mol Cell Biol*. 2006;7:359–371.
54. Antonetti DA, Barber AJ, Khin S, Lieth E, Tarbell JM, Gardner TW. Vascular permeability in experimental diabetes is associated with reduced endothelial occludin content: vascular endothelial growth factor decreases occludin in retinal endothelial cells. Penn State Retina Research Group. *Diabetes*. 1998;47:1953–1959.
55. Vinores SA, Derevjanik NL, Ozaki H, Okamoto N, Campochiaro PA. Cellular mechanisms of blood-retinal barrier dysfunction in macular edema. *Doc Ophthalmol*. 1999;97: 217–228.
56. Ristori C, Filippi L, Dal Monte M, et al. Role of the adrenergic system in a mouse model of oxygen-induced retinopathy: antiangiogenic effects of beta-adrenoreceptor blockade. *Invest Ophthalmol Vis Sci*. 2011;52:155–170.
57. Sennlaub F, Courtois Y, Goureau O. Inducible nitric oxide synthase mediates retinal apoptosis in ischemic proliferative retinopathy. *J Neurosci*. 2002;22:3987–3993.
58. Liang X, Zhou H, Ding Y, et al. TMP prevents retinal neovascularization and imparts neuroprotection in an oxygen-induced retinopathy model. *Invest Ophthalmol Vis Sci*. 2012;53:2157–2169.
59. Kaur C, Rathnasamy G, Ling EA. Roles of activated microglia in hypoxia induced neuroinflammation in the developing brain and the retina. *J Neuroimmune Pharmacol*. 2013;8:66–78.
60. Wang M, Ma W, Zhao L, Fariss RN, Wong WT. Adaptive Müller cell responses to microglial activation mediate neuroprotection and coordinate inflammation in the retina. *J Neuroinflammation*. 2011;8:173.
61. Staton CA, Reed MW, Brown NJ. A critical analysis of current in vitro and in vivo angiogenesis assays. *Int J Exp Pathol*. 2009; 90:195–221.
62. Vlieghe P, Lisowski V, Martinez J, Khrestchatisky M. Synthetic therapeutic peptides: science and market. *Drug Discov Today*. 2010;15:40–56.
63. Urtti A. Challenges and obstacles of ocular pharmacokinetics and drug delivery. *Adv Drug Deliv Rev*. 2006;58:1131–1135.
64. Bai Y, Zhao M, Zhang C, et al. Anti-angiogenic effects of a mutant endostatin: a new prospect for treating retinal and choroidal neovascularization. *PLoS One*. 2014;9:e112448.
65. Poettler M, Unseld M, Mihaly-Bison J. The urokinase receptor (CD87) represents a central mediator of growth factor-induced endothelial cell migration. *Thromb Haemost*. 2012;108:357–366.
66. Le Gat L, Gogat K, Bouquet C, et al. In vivo adenovirus-mediated delivery of a uPA/uPAR antagonist reduces retinal neovascularization in a mouse model of retinopathy. *Gene Ther*. 2003;10:2098–2103.
67. Muthusamy A, Lin CM, Shanmugam S, Lindner HM, Abcouwer SF, Antonetti DA. Ischemia-reperfusion injury induces occludin phosphorylation/ubiquitination and retinal vascular permeability in a VEGFR-2-dependent manner. *J Cereb Blood Flow Metab*. 2014;34:522–531.
68. Larusch GA, Merkulova A, Mahdi F, et al. Domain 2 of uPAR regulates single-chain urokinase-mediated angiogenesis through β1-integrin and VEGFR2. *Am J Physiol Heart Circ Physiol*. 2013;305:H305–H320.
69. Fong GH. Regulation of angiogenesis by oxygen sensing mechanisms. *J Mol Med*. 2009;87:549–560.
70. Chen Z, Han ZC. STAT3: a critical transcription activator in angiogenesis. *Med Res Rev*. 2008;28:185–200.
71. Oellerich T, Oellerich MF, Engelke M, et al. β2 integrin-derived signals induce cell survival and proliferation of AML blasts by activating a Syk/STAT signaling axis. *Blood*. 2013;121:3889–3899.
72. El-Remessy AB, Franklin T, Ghaley N, et al. Diabetes-induced superoxide anion and breakdown of the blood-retinal barrier: role of the VEGF/uPAR pathway. *PLoS One*. 2013;8:e71868.
73. El-Remessy AB, Behzadian MA, Abou-Mohamed G, Franklin T, Caldwell RW, Caldwell RB. Experimental diabetes causes breakdown of the blood-retina barrier by a mechanism involving tyrosine nitration and increases in expression of vascular endothelial growth factor and urokinase plasminogen activator receptor. *Am J Pathol*. 2003;162:1995–2004.
74. Downie LE, Pianta MJ, Vingrys AJ, Wilkinson-Berka JL, Fletcher EL. Neuronal and glial cell changes are determined by retinal vascularization in retinopathy of prematurity. *J Comp Neurol*. 2007;504:404–417.
75. Akula JD, Hansen RM, Martinez-Perez ME, Fulton AB. Rod photoreceptor function predicts blood vessel abnormality in retinopathy of prematurity. *Invest Ophthalmol Vis Sci*. 2007; 48:4351–4359.
76. Akula JD, Hansen RM, Tzekov R, et al. Visual cycle modulation in neurovascular retinopathy. *Exp Eye Res*. 2010;91:153–161.
77. Hatzopoulos KM, Vessey KA, Wilkinson-Berka JL, Fletcher EL. The vasoneuronal effects of AT1 receptor blockade in a rat model of retinopathy of prematurity. *Invest Ophthalmol Vis Sci*. 2014;55:3957–3970.
78. Gaucher D, Chiappore JA, Pâques M. Microglial changes occur without neural cell death in diabetic retinopathy. *Vision Res*. 2007;47:612–623.
79. Reichenbach A, Wurm A, Pannicke T, Iandiev I, Wiedemann P, Bringmann A. Müller cells as players in retinal degeneration and edema. *Graefes Arch Clin Exp Ophthalmol*. 2007;245: 627–636.
80. Newman EA. Müller cells and the retinal pigment epithelium. In: Albert DM, Jakobiec FA, eds. *Principles and Practice of Ophthalmology*. Philadelphia: Saunders; 2000:1763–1785.
81. Ishizuka F, Shimazawa M, Egashira Y, et al. Cilostazol prevents retinal ischemic damage partly via inhibition of tumor necrosis factor-α-induced nuclear factor-kappa B/activator protein-1 signaling pathway. *Pharmacol Res Perspect*. 2013;1:e00006.
82. Abcouwer SF, Gardner TW. Diabetic retinopathy: loss of neuroretinal adaptation to the diabetic metabolic environment. *Ann N Y Acad Sci*. 2014;1311:174–190.
83. García C, Aranda J, Arnold E, et al. Vasoinhibins prevent retinal vasopermeability associated with diabetic retinopathy in rats via protein phosphatase 2A-dependent eNOS inactivation. *J Clin Invest*. 2008;118:2291–2300.